Epigenome changes in active and inactive Polycomb-group-controlled regions. EMBO Rep. **5**:976–982.
9. **Bruggeman, S. W., M. E. Valk-Lingbeek, P. P. van der Stoop, J. J. Jacobs, K. Kieboom, E. Tanger, D. Hulsman, C. Leung, Y. Arsenijevic, S. Marino, and M. van Lohuizen.** 2005. Ink4a and Arf differentially affect cell proliferation and neural stem cell self-renewal in Bmi1-deficient mice. Genes Dev. **19**: 1438–1443.
10. **Buchwald, G., P. van der Stoop, O. Weichenrieder, A. Perrakis, M. van Lohuizen, and T. K. Sixma.** 2006. Structure and E3-ligase activity of the Ring-Ring complex of Polycomb proteins Bmi1 and Ring1b. EMBO J. **25**: 2465–2474.
11. **Buszczak, M., and A. C. Spradling.** 2006. Searching chromatin for stem cell identity. Cell **125**:233–236.
12. **Cao, R., L. Wang, H. Wang, L. Xia, H. Erdjument-Bromage, P. Tempst, R. S. Jones, and Y. Zhang.** 2002. Role of histone H3 lysine 27 methylation in Polycomb-group silencing. Science **298**:1039–1043.
13. **Cooper, A. B., C. M. Sawai, E. Sicinska, S. E. Powers, P. Sicinski, M. R. Clark, and I. Aifantis.** 2006. A unique function for cyclin D3 in early B cell development. Nat. Immunol. **7**:489–497.
14. **Coré, N., F. Joly, A. Boned, and M. Djabali.** 2004. Disruption of E2F signaling suppresses the INK4a-induced proliferative defect in M33-deficient mice. Oncogene **23**:7660–7668.
15. **Coré, N., S. Bel, S. J. Gaunt, M. Aurrand-Lions, J. Pearce, A. Fisher, and M. Djabali.** 1997. Altered cellular proliferation and mesoderm patterning in Polycomb-M33-deficient mice. Development **124**:721–729.
16. **Cozzio, A., E. Passegué, P. M. Ayton, H. Karsunky, M. L. Cleary, and I. L. Weissman.** 2003. Similar MLL-associated leukemias arising from self-renewing stem cells and short-lived myeloid progenitors. Genes Dev. **17**:3029–3035.
17. **Crosnier, C., D. Stamataki, and J. Lewis.** 2006. Organizing cell renewal in the intestine: stem cells, signals and combinatorial control. Nat. Rev. Genet. **7**:349–359.
18. **Czermin, B., R. Melfi, D. McCabe, V. Seitz, A. Imhof, and V. Pirrotta.** 2002. *Drosophila* enhancer of Zeste/ESC complexes have a histone H3 methyltransferase activity that marks chromosomal Polycomb sites. Cell **111**:185–196.
19. **del Mar Lorente, M., C. Marcos-Gutiérrez, C. Pérez, J. Schoorlemmer, A. Ramírez, T. Magin, and M. Vidal.** 2000. Loss- and gain-of-function mutations show a Polycomb group function for Ring1A in mice. Development **127**:5093–5100.
20. **de Napoles, M., J. E. Mermoud, R. Wakao, Y. A. Tang, M. Endoh, R. Appanah, T. B. Nesterova, J. Silva, A. P. Otte, M. Vidal, H. Koseki, and N. Brockdorff.** 2004. Polycomb group proteins Ring1A/B link ubiquitylation of histone H2A to heritable gene silencing and X inactivation. Dev. Cell **7**:663–676.
21. **Dietrich, N., A. P. Bracken, E. Trinh, C. K. Schjerling, H. Koseki, J. Rappsilber, K. Helin, and K. H. Hansen.** 2007. Bypass of senescence by the polycomb group protein CBX8 through direct binding to the INK4A-ARF locus. EMBO J. **26**:1637–1648.
22. **Gearhart, M. D., C. M. Corcoran, J. A. Wamstad, and V. J. Bardwell.** 2006. Polycomb group and SCF ubiquitin ligases are found in a novel BCOR complex that is recruited to BCL6 targets. Mol. Cell. Biol. **26**:6880–6889.
23. **Gil, J., and G. Peters.** 2006. Regulation of the INK4b-ARF-INK4a tumour suppressor locus: all for one or one for all. Nat. Rev. Mol. Cell Biol. **7**:667–677.
24. **Glinsky, G. V., O. Berezovska, and A. B. Glinskii.** 2005. Microarray analysis identifies a death-from-cancer signature predicting therapy failure in patients with multiple types of cancer. J. Clin. Investig. **115**:1503–1521.
25. **Hemenway, C. S., B. W. Halligan, and L. S. Levy.** 1998. The Bmi-1 oncoprotein interacts with dinG and MPh2: the role of RING finger domains. Oncogene **16**:2541–2547.
26. **Hosen, N., T. Yamane, M. Muijtjens, K. Pham, M. F. Clarke, and I. L. Weissman.** 2007. Bmi-1-green fluorescent protein-knock-in mice reveal the dynamic regulation of bmi-1 expression in normal and leukemic hematopoietic cells. Stem Cells **25**:1635–1644.
27. **Jacobs, J. J., B. Scheijen, J. W. Voncken, K. Kieboom, A. Berns, and M. van Lohuizen.** 1999. Bmi-1 collaborates with c-Myc in tumorigenesis by inhibiting c-Myc-induced apoptosis via INK4a/ARF. Genes Dev. **13**:2678–2690.
28. **Kajiume, T., Y. Ninomiya, H. Ishihara, R. Kanno, and M. Kanno.** 2004. Polycomb group gene mel-18 modulates the self-renewal activity and cell cycle status of hematopoietic stem cells. Exp. Hematol. **32**:571–578.
29. **Kato, Y., H. Koseki, M. Vidal, H. Nakauchi, and A. Iwama.** 2007. Unique composition of polycomb repressive complex 1 in hematopoietic stem cells. Int. J. Hematol. **85**:179–181.
30. **Kondo, M., I. L. Weissman, and K. Akashi.** 1997. Identification of clonogenic common lymphoid progenitors in mouse bone marrow. Cell **91**:661–672.
31. **Kotake, Y., R. Cao, P. Viatour, J. Sage, Y. Zhang, and Y. Xiong.** 2007. pRB family proteins are required for H3K27 trimethylation and Polycomb repression complexes binding to and silencing $p16^{INK4a}$ tumor suppressor gene. Genes Dev. **21**:49–54.
32. **Krivtsov, A. V., D. Twomey, Z. Feng, M. C. Stubbs, Y. Wang, J. Faber, J. E. Levine, J. Wang, W. C. Hahn, D. G. Gilliland, T. R. Golub, and S. A. Armstrong.** 2006. Transformation from committed progenitor to leukaemia stem cell initiated by MLL-AF9. Nature **442**:818–822.
33. **Kühn, R., F. Schwenk, M. Aguet, and K. Rajewsky.** 1995. Inducible gene targeting in mice. Science **269**:1427–1429.
34. **Kuzmichev, A., K. Nishioka, H. Erdjument-Bromage, P. Tempst, and D. Reinberg.** 2002. Histone methyltransferase activity associated with a human multiprotein complex containing the Enhancer of Zeste protein. Genes Dev. **16**:2893–2905.
35. **Lessard, J., A. Schumacher, U. Thorsteinsdottir, M. van Lohuizen, T. Magnuson, and G. Sauvageau.** 1999. Functional antagonism of the Polycomb-group genes Eed and Bmi1 in hemopoietic cell proliferation. Genes Dev. **13**:2691–2703.
36. **Lessard, J., and G. Sauvageau.** 2003. Polycomb group genes as epigenetic regulators of normal and leukemic hemopoiesis. Exp. Hematol. **31**:567–585.
37. **Lessard, J., and G. Sauvageau.** 2003. Bmi-1 determines the proliferative capacity of normal and leukaemic stem cells. Nature **423**:255–260.
38. **Leung, C., M. Lingbeek, O. Shakhova, J. Liu, E. Tanger, P. Saremaslani, M. Van Lohuizen, and S. Marino.** 2004. Bmi1 is essential for cerebellar development and is overexpressed in human medulloblastomas. Nature **428**:337–341.
39. **Levine, S. S., A. Weiss, H. Erdjument-Bromage, Z. Shao, P. Tempst, and R. E. Kingston.** 2002. The core of the Polycomb repressive complex is compositionally and functionally conserved in flies and humans. Mol. Cell. Biol. **22**:6070–6078.
40. **Levine, S. S., I. F. King, and R. E. Kingston.** 2004. Division of labor in Polycomb group repression. Trends Biochem. Sci. **29**:478–485.
41. **Martinez, A. M., and G. Cavalli.** 2006. The role of Polycomb group proteins in cell cycle regulation during development. Cell Cycle **5**:1189–1197.
42. **Martinez, A. M., S. Colomb, J. Déjardin, F. Bantignies, and G. Cavalli.** 2006. Polycomb group-dependent cyclin A repression in *Drosophila*. Genes. Dev. **20**:501–513.
43. **Mijimolle, N., J. Velasco, P. Dubus, C. Guerra, C. A. Weinbaum, P. J. Casey, V. Campuzano, and M. Barbacid.** 2005. Protein farnesyltransferase in embryogenesis, adult homeostasis, and tumor development. Cancer Cell **7**:313–324.
44. **Molofsky, A. V., R. Pardal, T. Iwashita, I. K. Park, M. F. Clarke, and S. J. Morrison.** 2003. Bmi-1 dependence distinguishes neural stem cell self-renewal from progenitor proliferation. Nature **425**:962–967.
45. **Molofsky, A. V., S. He, M. Bydon, S. J. Morrison, and R. Pardal.** 2005. Bmi-1 promotes neural stem cell self-renewal and neural development but not mouse growth and survival by repressing the $p16^{Ink4a}$ and $p19^{Arf}$ senescence pathways. Genes Dev. **19**:1432–1437.
46. **Müller, J., C. M. Hart, N. J. Francis, M. L. Vargas, A. Sengupta, B. Wild, E. L. Miller, M. B. O'Connor, R. E. Kingston, and J. A. Simon.** 2002. Histone methyltransferase activity of a *Drosophila* Polycomb group repressor complex. Cell **111**:197–208.
47. **Ogawa, H., K. Ishiguro, S. Gaubatz, D. M. Livingston, and Y. Nakatani.** 2002. A complex with chromatin modifiers that occupies E2F- and Myc-responsive genes in G0 cells. Science **296**:1132–1136.
48. **Oguro, H., A. Iwama, Y. Morita, T. Kamijo, M. van Lohuizen, and H. Nakauchi.** 2006. Differential impact of Ink4a and Arf on hematopoietic stem cells and their bone marrow microenvironment in Bmi1-deficient mice. J. Exp. Med. **203**:2247–2253.
49. **Ohta, H., A. Sawada, J. Y. Kim, S. Tokimasa, S. Nishiguchi, R. K. Humphries, J. Hara, and Y. Takihara.** 2002. Polycomb group gene rae28 is required for sustaining activity of hematopoietic stem cells. J. Exp. Med. **195**:759–770.
50. **Papp, B., and J. Müller.** 2006. Histone trimethylation and the maintenance of transcriptional ON and OFF states by TrxG and PcG proteins. Genes. Dev. **20**:2041–2054.
51. **Park, I. K., D. Qian, M. Kiel, M. W. Becker, M. Pihalja, I. L. Weissman, S. J. Morrison, and M. F. Clarke.** 2003. Bmi-1 is required for maintenance of adult self-renewing haematopoietic stem cells. Nature **423**:302–305.
52. **Pasini, D., A. P. Bracken, and K. Helin.** 2004. Polycomb group proteins in cell cycle progression and cancer. Cell Cycle **3**:396–400.
53. **Passegué, E., A. J. Wagers, S. Giuriato, W. C. Anderson, and I. L. Weissman.** 2005. Global analysis of proliferation and cell cycle gene expression in the regulation of hematopoietic stem and progenitor cell fates. J. Exp. Med. **202**:1599–1611.
54. **Raaphorst, F. M.** 2005. Deregulated expression of Polycomb-group oncogenes in human malignant lymphomas and epithelial tumors. Hum. Mol. Genet. **14**(Suppl. 1):R93–R100.
55. **Raaphorst, F. M., A. P. Otte, and C. J. Meijer.** 2001. Polycomb-group genes as regulators of mammalian lymphopoiesis. Trends Immunol. **22**:682–690.
56. **Rando, T. A.** 2006. Stem cells, ageing and the quest for immortality. Nature **441**:1080–1086.
57. **Ringrose, L., and R. Paro.** 2004. Epigenetic regulation of cellular memory by the polycomb and trithorax group proteins. Annu. Rev. Genet. **38**:413–443.
58. **Rosenbauer, F., and D. G. Tenen.** 2007. Transcription factors in myeloid development: balancing differentiation with transformation. Nat. Rev. Immunol. **7**:105–117.
59. **Sánchez, C., I. Sánchez, J. A. Demmers, P. Rodriguez, J. Strouboulis, and M.**

**Vidal.** 2007. Proteomic analysis of Ring1B/Rnf2 interactors identifies a novel complex with the Fbxl10/ Jmjd1B histone demethylase and the BcoR corepressor. Mol. Cell. Proteomics **6**:820–834.
60. **Sánchez-Beato, M., E. Sánchez, J. González-Carreró, M. Morente, A. Diez, L. Sánchez-Verde, M. C. Martín, J. C. Cigudosa, M. Vidal, and M. A. Piris.** 2006. Variability in the expression of polycomb proteins in different normal and tumoral tissues. A pilot study using tissue microarrays. Mod. Pathol. **19**:684–694.
61. **Sasaki, Y., C. T. Jensen, S. Karlsson, and S. E. Jacobsen.** 2004. Enforced expression of cyclin D2 enhances the proliferative potential of myeloid progenitors, accelerates in vivo myeloid reconstitution, and promotes rescue of mice from lethal myeloablation. Blood **104**:986–992.
62. **Schmitt, C. A., M. E. McCurrach, E. de Stanchina, R. R. Wallace-Brodeur, and S. W. Lowe.** 1999. INK4a/ARF mutations accelerate lymphomagenesis and promote chemoresistance by disabling p53. Genes. Dev. **13**:2670–2677.
63. **Schoorlemmer, J., C. Marcos-Gutiérrez, F. Were, R. Martínez, E. García, D. P. Satijn, A. P. Otte, and M. Vidal.** 1997. Ring1A is a transcriptional repressor that interacts with the Polycomb-M33 protein and is expressed at rhombomere boundaries in the mouse hindbrain. EMBO J. **16**:5930–5942.
64. **Schuettengruber, B., D. Chourrout, M. Vervoort, B. Leblanc, and G. Cavalli.** 2007. Genome regulation by polycomb and trithorax proteins. Cell **128**:735–745.
65. **Serrano, M., H. Lee, L. Chin, C. Cordon-Cardo, D. Beach, and R. A. DePinho.** 1996. Role of the INK4a locus in tumor suppression and cell mortality. Cell **85**:27–37.
66. **Sherr, C. J., and J. M. Roberts.** 1999. CDK inhibitors: positive and negative regulators of G1-phase progression. Genes Dev. **13**:1501–1512.
67. **Soriano, P.** 1997. The PDGF alpha receptor is required for neural crest cell development and for normal patterning of the somites. Development **124**: 2691–2700.
68. **Sparmann, A., and M. van Lohuizen.** 2006. Polycomb silencers control cell fate, development and cancer. Nat. Rev. Cancer. **6**:846–856.
69. **Takihara, Y., D. Tomotsune, M. Shirai, Y. Katoh-Fukui, K. Nishii, M. A. Motaleb, M. Nomura, R. Tsuchiya, Y. Fujita, Y. Shibata, T. Higashinakagawa, and K. Shimada.** 1997. Targeted disruption of the mouse homologue of the *Drosophila* polyhomeotic gene leads to altered anteroposterior patterning and neural crest defects. Development **124**:3673–3682.
70. **Tokimasa, S., H. Ohta, A. Sawada, Y. Matsuda, J. Y. Kim, S. Nishiguchi, J. Hara, and Y. Takihara.** 2001. Lack of the Polycomb-group gene rae28 causes maturation arrest at the early B-cell developmental stage. Exp. Hematol. **29**:93–103.
71. **van der Lugt, N. M., J. Domen, K. Linders, M. van Roon, E. Robanus-Maandag, H. te Riele, M. van der Valk, J. Deschamps, M. Sofroniew, and M. van Lohuizen.** 1994. Posterior transformation, neurological abnormalities, and severe hematopoietic defects in mice with a targeted deletion of the *bmi-1* proto-oncogene. Genes Dev. **8**:757–769.
72. **Voncken, J. W., B. A. Roelen, M. Roefs, S. de Vries, E. Verhoeven, S. Marino, J. Deschamps, and M. van Lohuizen.** 2003. Rnf2 (Ring1b) deficiency causes gastrulation arrest and cell cycle inhibition. Proc. Natl. Acad. Sci. USA **100**:2468–2473.
73. **Wang, H., L. Wang, H. Erdjument-Bromage, M. Vidal, P. Tempst, R. S. Jones, and Y. Zhang.** 2004. Role of histone H2A ubiquitination in Polycomb silencing. Nature **431**:873–878.
74. **Weissman, I. L.** 2000. Stem cells: units of development, units of regeneration, and units in evolution. Cell **100**:157–168.

nature genetics



# PRC1 and Suv39h specify parental asymmetry at constitutive heterochromatin in early mouse embryos

Mareike Puschendorf[1], Rémi Terranova[1], Erwin Boutsma[2], Xiaohong Mao[3,6], Kyo-ichi Isono[4], Urszula Brykczynska[1], Carolin Kolb[1], Arie P Otte[5], Haruhiko Koseki[4], Stuart H Orkin[3], Maarten van Lohuizen[2] & Antoine H F M Peters[1]

**In eukaryotes, *Suv39h* H3K9 trimethyltransferases are required for pericentric heterochromatin formation and function. In early mouse preimplantation embryos, however, paternal pericentric heterochromatin lacks *Suv39h*-mediated H3K9me3 and downstream marks. Here we demonstrate *Ezh2*-independent targeting of maternally provided polycomb repressive complex 1 (PRC1) components to paternal heterochromatin. In *Suv39h2* maternally deficient zygotes, PRC1 also associates with maternal heterochromatin lacking H3K9me3, thereby revealing hierarchy between repressive pathways. In *Rnf2* maternally deficient zygotes, the PRC1 complex is disrupted, and levels of pericentric major satellite transcripts are increased at the paternal but not the maternal genome. We conclude that in early embryos, *Suv39h*-mediated H3K9me3 constitutes the dominant maternal transgenerational signal for pericentric heterochromatin formation. In absence of this signal, PRC1 functions as the default repressive back-up mechanism. Parental epigenetic asymmetry, also observed along cleavage chromosomes, is resolved by the end of the 8-cell stage—concurrent with blastomere polarization—marking the end of the maternal-to-embryonic transition.**

In mammals, parental genomes are epigenetically distinct, despite their genetic resemblance[1]. During early mouse preimplantation development, parental genomes are highly asymmetric in epigenetic modifications of DNA and associated chromatin[2–9]. At gamete fusion, the maternal genome exists in a nucleosomal configuration marked by distinct types of histone lysine methylation inherited from the oocyte. In contrast, following the histone-to-protamine exchange occurring during spermiogenesis, the paternal genome incorporates maternally provided histones and becomes *de novo* methylated at different lysine residues in a highly spatially and temporally coordinated manner. The function of parental epigenetic asymmetry for gene expression and genome reorganization[6,10] is largely enigmatic, as are the mechanisms of establishment, maintenance and resolution. A key question is whether parentally inherited epigenetic states affect *de novo* targeting and function of (maternally provided) epigenetic modifiers in *cis* and/or in *trans* in the early embryo, thereby directing gene expression over shorter or longer developmental time windows. Notably, transmission of the paternal genome in a nucleosomal state impairs DNA methylation reprogramming in early embryos[11]. Here, we study the transgenerational contribution of two distinct evolutionarily conserved classes of epigenetic modifiers in defining parental asymmetry at constitutive heterochromatin and euchromatin in preimplantation embryos.

The first class consists of the Suv39h histone methyltransferases (HMTs), which are essential for constitutive heterochromatin formation and function, gene repression and maintenance of genome integrity[12–15]. *Suv39h*-mediated H3K9me3 directs chromatin binding of the heterochromatic proteins HP1α, HPβ and HPγ (ref. 16), which target the two H4K20 di- and trimethylation-specific Suv4-20h HMTs and the Dnmt3a/3b DNA methyltransferases, to establish a transcriptionally repressed state[17–19].

The second class consists of Polycomb group (PcG) proteins, which are repressive chromatin factors required for maintaining cell identity[14,20]. PcG proteins are classified into two groups of multimeric protein complexes termed polycomb repressive complexes (PRCs). In *Drosophila melanogaster*, PRC1 contains four core components for which multiple paralogs exist in mammals[21]. *In vitro*, PRC1 mediates repression by inhibiting chromatin remodeling, impairing the transcription machinery and by mediating chromatin compaction[22]. The mammalian and fly RING orthologs function as E3 ubiquitin ligases that monoubiquitinate H2A at lysine 119, a modification associated with gene repression[23,24]. PRC2 consists of Ezh2, Suz12 and Eed, which

[1]Friedrich Miescher Institute for Biomedical Research, Maulbeerstrasse 66, CH-4058 Basel, Switzerland. [2]Division of Molecular Genetics and Centre for Biomedical Genetics, The Netherlands Cancer Institute, Plesmanlaan 121, 1066 CX Amsterdam, The Netherlands. [3]Department of Pediatric Oncology, Dana Farber Cancer Institute, Harvard Stem Cell Institute and Howard Hughes Medical Institute, Harvard Medical School, Boston, Massachusetts 02115, USA. [4]RIKEN Research Center for Allergy and Immunology, RIKEN Yokohama Institute, 1-7-22 Suehiro-cho, Tsurumi-ku Yokohama City, Kanagawa 230-0045, Japan. [5]Swammerdam Institute for Life Sciences, University of Amsterdam, Kruislaan 406, 1098 SM Amsterdam, The Netherlands. [6]Present address: Novartis Institutes for BioMedical Research, Inc., 250 Massachusetts Avenue, Cambridge, Massachusetts 02139, USA. Correspondence should be addressed to A.H.F.M.P. (antoine.peters@fmi.ch).

Received 14 November 2007; accepted 22 January 2008; published online 2 March 2008; corrected online 16 March 2008 (details online); doi:10.1038/ng.99

together mediate H3K27me2 and H3K27me3 (H3K27me2/3)[21,25]. Genome-wide chromatin profiling has shown that components of PRC1 and PRC2 co-occupy promoters of genes enriched in H3K27me3 (ref. 26). At selected genes, PRC2 is required for binding of PRC1 (ref. 26), suggesting that PRC1 can be targeted via mammalian orthologs of *Drosophila* Polycomb that bind H3K27me3 (refs. 27,28). In *Eed*$^{-/-}$ embryonic stem cells, most joint targets of PRC1 and PRC2 are transcriptionally activated[26].

In this study, we addressed the parental influence on constitutive heterochromatin formation in early mouse embryos. In zygotes, only maternal constitutive heterochromatin is labeled by HP1β and H3K9me2/3 marks inherited from the oocyte[2,6,7,9]. We investigated whether absence of the *Suv39h*-dependent chromatin signature at paternal constitutive heterochromatin is compensated by targeting of other repressive histone modifications and/or proteins. We show that H3K27me2/3 and PRC1 components accumulate at paternal heterochromatin. In contrast to promoters of certain developmental regulators[26], PRC1 targeting to heterochromatin is independent of PRC2 function. PRC1 is required for transcriptional repression of heterochromatic major satellite repeats. We further demonstrate that parental-specific *Suv39h* and PRC1-defined states are inherited over the first three cleavage divisions and that asymmetry is not limited to constitutive heterochromatin only. Finally, we explain the basic principle underlying parental origin–specific definition of constitutive heterochromatin by Suv39h and Polycomb-based repression mechanisms.

## RESULTS

### PRC1 components define paternal heterochromatin

In mouse somatic cells, pericentric heterochromatin of different chromosomes cluster into chromocenters that can be visualized by fluorochromes such as 4,6-diamidino-2-phenylindole (DAPI) that preferentially bind to the underlying AT-rich major satellite sequences[29]. In zygotes, DAPI-intense chromatin is organized into ring structures around nucleolar-precursor bodies (NPBs)[6]. By DNA FISH for major satellites, we show that pericentric heterochromatin co-localizes with DAPI-intense rings around NPBs (**Fig. 1a**)[30]. Centromeric minor satellite foci are interspersed within major satellites (**Fig. 1a**)[30]. We confirm that in zygotes, only maternal constitutive heterochromatin is labeled by H3K9me3 and H4K20me3 (**Fig. 1b** and **Supplementary Fig. 1** online)[2,6,7,9], two modifications that are inherited from the oocyte. HP1β is loaded onto maternal heterochromatin upon gamete fusion (**Fig. 1b** and **Supplementary Fig. 1**).

In embryonic stem cells, pericentric heterochromatin acquires H3K27me3 in the absence of the *Suv39h*-mediated chromatin configuration[31]. To determine whether such a compensatory mechanism also operates in early embryos, we analyzed H3K27 methylation states in late zygotes. Indeed, H3K27me2/3 modifications were

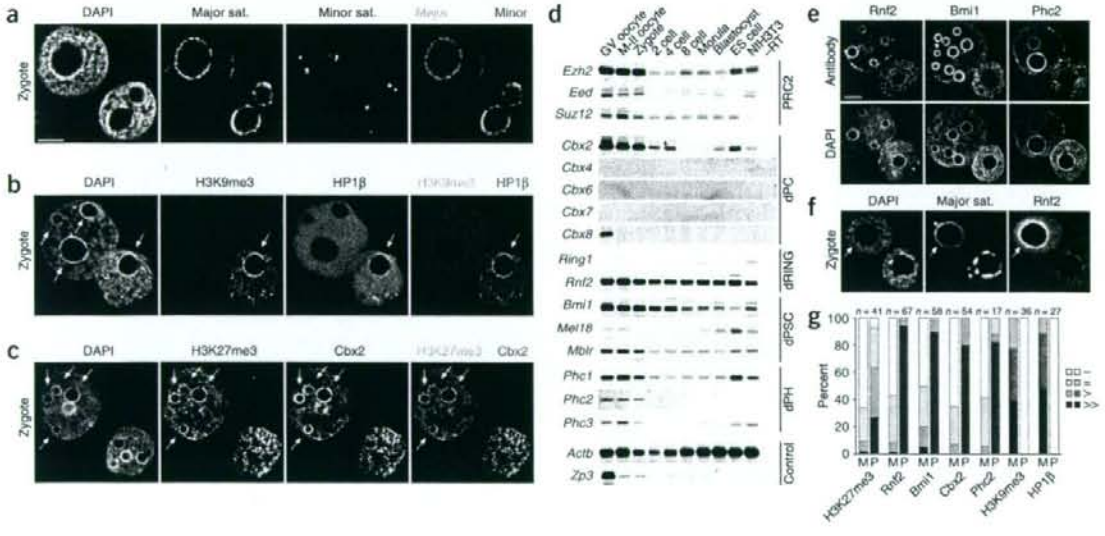


**Figure 1** Maternal and paternal heterochromatin are marked by distinct repressive complexes in preimplantation embryos. (**a**) DNA-FISH analysis showing localization of major satellite and minor satellite sequences along DAPI-intense ring structures around NPBs in late mouse zygotes. (**b**) Immunofluorescence analysis of late zygotes showing euchromatic localization of HP1β in the large paternal pronucleus (left) and genome-wide H3K9me3 and HP1β staining in the maternal pronucleus (right). Constitutive heterochromatin (arrows) is only maternally labeled by H3K9me3 and HP1β. (**c**) Immunofluorescence analysis of late zygotes showing euchromatic staining of H3K27me3 and Cbx2 in both pronuclei. Constitutive heterochromatin is only paternally labeled by H3K27me3 and Cbx2 (arrows). (**d**) RT-PCR analysis of PRC2 and PRC1 components in oocytes and preimplantation embryos. RNA from embryonic stem cells and NIH3T3 cells was used as control. –RT refers to analysis of M-II oocytes without reverse transcriptase. Ubiquitously expressed β-actin (*Actb*) and oocyte-restricted zona pellucida 3 (*Zp3*) serve as controls. For mouse PRC1 genes, *Drosophila* orthologs are given on the right. (**e**) Immunofluorescence analysis of late zygotes showing heterochromatic enrichment of Rnf2, Bmi1 and Phc2 paternally only. All three proteins label euchromatin of both pronuclei. (**f**) Co-immuno-DNA-FISH analysis showing co-localization of major satellite sequences with Rnf2 in the paternal pronucleus (arrow). (**g**) Levels of enrichment of H3K9me3, HP1β, H3K27me3 and PRC1 components at maternal (M) versus paternal (P) constitutive heterochromatin in late zygotes were scored as follows: (–) no staining; (=) equal hetero- and euchromatic staining; (>) enhanced and (>>) strongly enhanced staining of heterochromatin versus euchromatin. Scale bars, 10 μm.

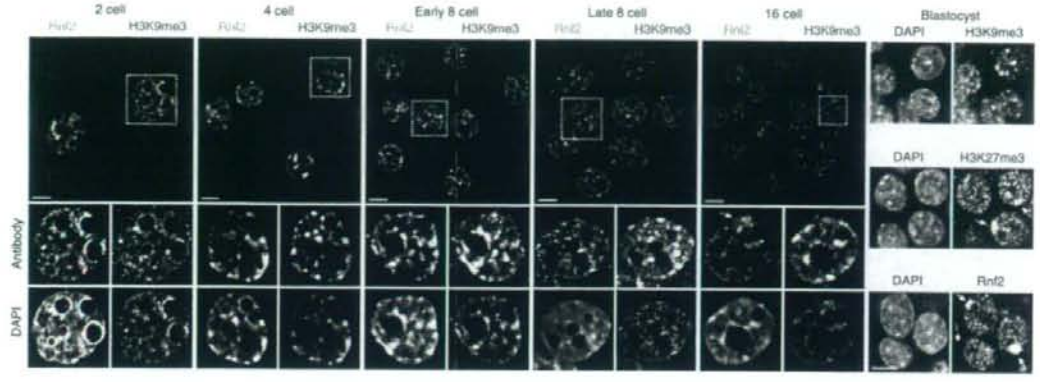


**Figure 2** Differential heterochromatic states are maintained up to the 8-cell stage in a parental origin–dependent manner. Immunofluorescence analyses of Rnf2 and H3K9me3 in 2-cell, 4-cell, early 8-cell (before compaction), late 8-cell (after compaction), 16-cell and blastocyst embryos. In 2-cell embryos, exclusive enrichment of either H3K9me3 or Rnf2 is detected at individual DAPI-intense heterochromatic chromocenters. Following the gradual intermingling of parental genomes, chromocenters become progressively doubly labeled by H3K9me3 and Rnf2. From the late 8-cell stage onwards, Rnf2 is completely replaced by H3K9me3 at heterochromatin. From the 16-cell stage onwards, Rnf2 is enriched at the presumptive inactive X chromosome (arrow) in female embryos. Scale bars, 20 μm. In blastocysts, H3K9me3 marks DAPI-intense chromocenters, whereas H3K27me3 and Rnf2 are enriched at the presumptive inactive X chromosome (arrows). Other matPRC1 components were not enriched (Phc2) or occasionally weakly enriched (Cbx2) at the inactive X (data not shown). Scale bar, 10 μm.

enriched at pericentric heterochromatin of paternal origin only (**Fig. 1c** and **Supplementary Fig. 1**), whereas the remainder of both parental genomes (referred to as 'euchromatin') was labeled by both marks[7]. H3K27me1 labeled euchromatin and was enriched at heterochromatin of both pronuclei (**Supplementary Fig. 1**). Therefore, H3K27me states define constitutive heterochromatin depending on parental descent.

To identify PcG complexes functioning in early embryos[21,25], we profiled RNA expression of PRC2 and PRC1 genes in oocytes and preimplantation embryos. For PRC2 components, we observed strong maternal and moderate zygotic expression (**Fig. 1d**). Similarly, at least one mammalian paralog of each *Drosophila* PRC1 core member was maternally and zygotically expressed (**Fig. 1d**). These data suggest that PRC2 and PRC1 have roles in preimplantation development.

We next asked whether H3K27me3 could, in principle, target PRC1 complexes to pericentric heterochromatin. We observed that, analogous to the binding of HP1β to H3K9me3[16], H3K27me3 co-localized with Cbx2 (**Fig. 1c**), a Polycomb protein known to bind to H3K27me3 via its chromodomain[27]. In addition, Rnf2 (Ring1b), Bmi1 and Phc2 also selectively accumulated at paternal constitutive heterochromatin (**Fig. 1e**), suggesting the presence of a functional 'maternally provided PRC1' complex ('matPRC1'). Immuno-DNA-FISH analysis confirmed co-localization of the matPRC1 complex with major satellites in the paternal genome (**Fig. 1f**). Euchromatin of both genomes was labeled by all four matPRC1 proteins as well as by Phc1 that was absent from paternal heterochromatin (data not shown). These data convincingly support a parental origin–dependent definition of constitutive heterochromatin (**Fig. 1g**).

### Parental-specific heterochromatic states are heritable

To investigate whether parental-specific heterochromatic states are transmitted, we profiled successive cleavage-stage embryos (**Fig. 2** and **Supplementary Fig. 2** online; $n$ = 15–25 per stage) in which

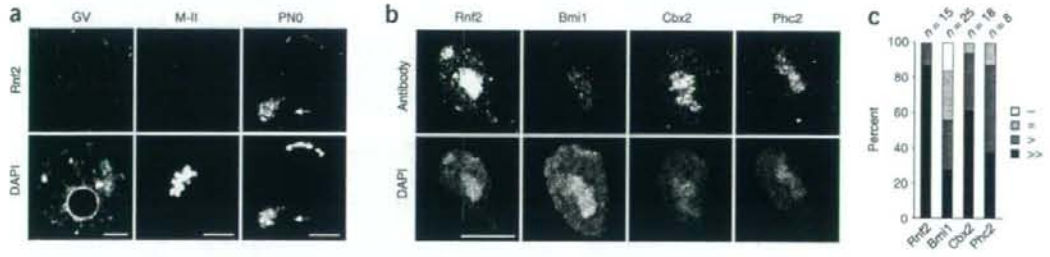


**Figure 3** PRC1 components are targeted to chromatin upon gamete fusion. (**a**) Immunofluorescence analyses of germinal vesicle (GV) and M-II oocytes and pronuclear stage 0 (PN0) zygotes show that Rnf2 starts to bind to the maternal genome shortly after gamete fusion. At PN0, the maternal genome is at anaphase of the 2nd meiotic division. The strongly labeled genome complement will constitute the embryo proper (bottom; arrow). The top set will segregate into the second polar body. Similar data were obtained for matPRC1 components Cbx2, Bmi1 and Phc2 (**Supplementary Fig. 4**). (**b**) Immunofluorescence analyses of matPRC1 enrichment at constitutive heterochromatin in decondensed sperm nuclei shortly after gamete fusion (PN0 stage). Constitutive heterochromatin is organized into one large chromocenter in most mature spermatozoa. (**c**) Numerical evaluation of data presented in **b** and **c**. Level of enrichment was scored as described in **Figure 1g**. Scale bars, 10 μm.

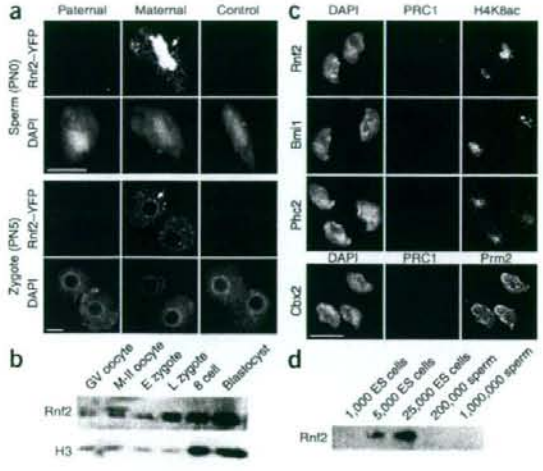


**Figure 4** Maternally provided Rnf2 is targeted to paternal constitutive heterochromatin and euchromatin. (**a**) Immunofluorescence analysis with antibodies to GFP shows binding of Rnf2–YFP fusion protein to paternal heterochromatin of decondensing spermatozoa and late zygotes only after maternal (arrows in middle panels) but not paternal (left panels) transmission of a functional Rnf2–YFP knock-in allele. Paternal and maternal euchromatin is also bound by maternal fusion protein (bottom middle panel). Scale bars, 10 μm. (**b**) Protein blot analysis of Rnf2 and histone H3 in germinal vesicle and M-II oocytes, in early (E) and late (L) zygotes, and in 8 cell and blastocyst embryos. Rnf2 protein levels strongly increased during the development of 1-cell embryos. We loaded 200 oocytes or embryos per lane. (**c**) Immunofluorescence analysis of isolated caudal epididymal spermatozoa shows labeling with H4K8ac and Protamine2 but not with PRC1 components. (**d**) Protein blot analysis of Rnf2 in isolated caudal epididymal spermatozoa and mouse embryonic stem cells fails to detect Rnf2 protein in 1,000,000 spermatozoa that are estimated to contain about 1% histones (U.B. and A.H.F.M.P., unpublished data), which is equivalent to the amount of histones present in 5,000 diploid embryonic stem cells.

heterochromatin becomes progressively reorganized and clustered into chromocenters[6]. In 2- and 4-cell embryos, individual DAPI-intense areas were labeled with either H3K9me3 (and HP1β) or matPRC1 components. Besides HP1β, HP1α and HP1γ were also associated to maternal H3K9me3-positive heterochromatin from the 4-cell stage onwards (data not shown). Following gradual intermingling of parental genomes[32], chromocenters became doubly labeled by H3K9me3 and Rnf2, particularly in early 8-cell embryos. Rnf2 association with pericentric heterochromatin strongly declined during the 8-cell stage and was completely replaced by H3K9me3 from the 16-cell stage onwards. At that point, Rnf2 started to accumulate at the presumptive Xi chromosome. In blastocysts, constitutive heterochromatin was labeled by H3K9me3 and HP1β ($n = 10$), whereas H3K27me3 and Rnf2 were enriched at facultative heterochromatin of the Xi ($n = 20–30$)[23].

To relate labeling of heterochromatin by Rnf2 versus H3K9me3 and HP1β to parental origin, we studied 4-cell embryos that were hybrid for the C57BL/6J and JF1 genetic backgrounds, which differ in DNA sequence composition at pericentric heterochromatin. By carrying out immuno-FISH using a probe specific for maternal C57BL/6J major satellites, we connected differential labeling of pericentric heterochromatin to parental origin (**Supplementary Fig. 3** online). We conclude

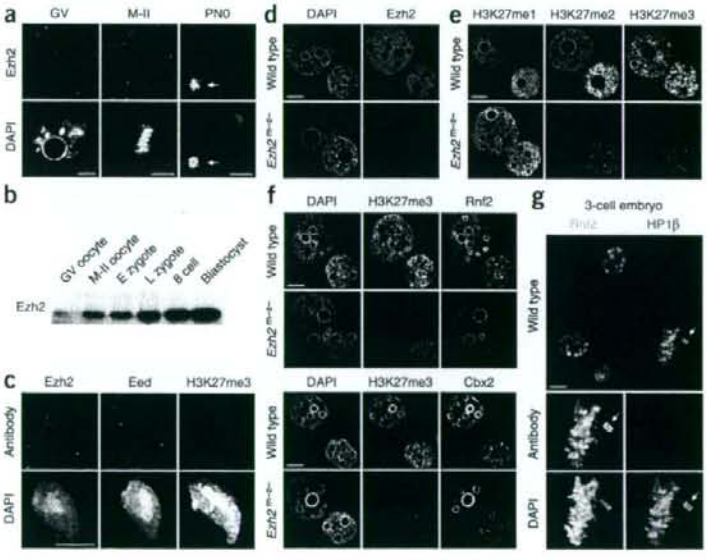


**Figure 5** Heterochromatic but not euchromatic matPRC1 targeting is *Ezh2* independent. (**a**) Immunofluorescence analysis of germinal vesicle and M-II oocytes and PN0 zygotes shows that after gamete fusion (PN0), Ezh2 preferentially accumulates at the maternal genome complement that will constitute the embryo (bottom; arrow). The top chromosome set will segregate into the second polar body. Similar data were obtained for Eed and Suz12 (**Supplementary Fig. 4**). (**b**) Protein blot analysis of Ezh2 in germinal vesicle and M-II oocytes, in early (E) and late (L) zygotes, and in 8 cell and blastocyst embryos show increasing Ezh2 protein levels from M-II stage onwards. Analyses were done on the same material as shown in **Figure 4b**. (**c**) Immunofluorescence analysis fails to show accumulation of Ezh2, Eed and H3K27me3 at DAPI-intense constitutive heterochromatin in decondensing sperm nuclei (PN0 stage). (**d**) Immunofluorescence analysis of wild-type and $Ezh2^{m-z-}$ late zygotes showing absence of Ezh2 protein upon maternal *Zp3*-cre mediated and paternal *Prm1*-cre mediated deletion. (**e**) Accordingly, the establishment and maintenance of H3K27me2 and H3K27me3 is impaired at paternal and maternal genomes in mutant zygotes, whereas H3K27me1 is unaffected. (**f**) Nevertheless, Rnf2 and Cbx2 localization to paternal heterochromatin is unaltered in $Ezh2^{m-z-}$ zygotes, whereas levels of euchromatic binding correlate with the level of H3K27me3. (**g**) Immunofluorescence analysis of a wild-type 3-cell embryo showing Rnf2 bound to interphase and mitotic chromatin, whereas HP1β is only bound to interphase chromatin. Arrow marks Rnf2 binding to mitotic chromosomes in a banded pattern. Scale bars in **a** and **c–f**, 10 μm. Scale bar in **g**, 20 μm.

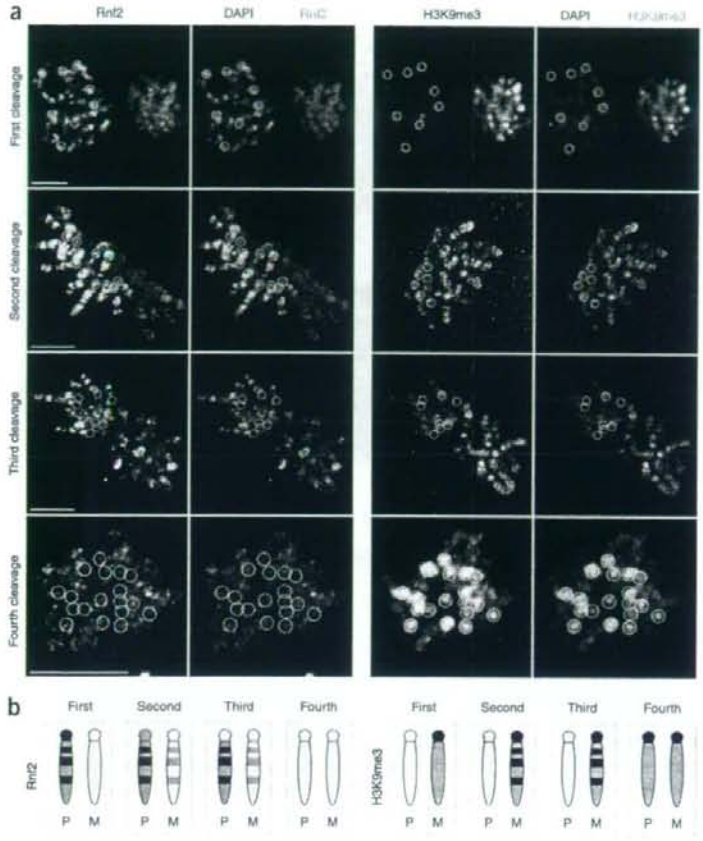


**Figure 6** Parent of origin–specific labeling of constitutive heterochromatin and chromosome arms by Rnf2 and H3K9me3. (**a**) Immunofluorescence analysis of pericentric heterochromatic regions of paternal prometaphase chromosomes (green circles) over successive cleavage divisions shows strong, moderate and weak Rnf2 enrichment at the first, second and third cleavage divisions, respectively. In contrast, maternal chromosome ends (red circles) are moderately enriched in H3K9me3 at all three divisions. At the subsequent fourth cleavage, all chromosomes ends (white circles) are strongly enriched in H3K9me3. During the first three cleavages, the arms of paternal and maternal chromosomes are also more intensely labeled by Rnf2 and H3K9me3 in a banded pattern, respectively. This parental-specific labeling of chromosome arms is lost at the fourth cleavage division. Before syngamy at the first cleavage, paternal and maternal chromosome sets are detected as separate entities. At the second and third cleavage divisions, parental chromosome sets are often not yet intermingled and lie adjacent to each other at the metaphase plate. Parental identity was assigned on the basis of levels of Rnf2 and H3K9me3 enrichment and position on the metaphase plate. Scale bars, 10 μm. (**b**) Graphical representation of the dynamics of asymmetric distribution of Rnf2 and H3K9me3 along paternal (P) and maternal (M) chromosomes at successive cleavage stages. Relative levels of enrichment are represented by color intensities. Stripes along chromosome arms represent banding patterns. Note that Rnf2 enrichment at paternal pericentric heterochromatin is progressively reduced at the second and third cleavages, whereas labeling along chromosome arms is not affected.



that the matPRC1-defined state at paternal constitutive heterochromatin is heritable over three consecutive cleavages and is subsequently replaced by the canonical *Suv39h*-mediated state.

### Paternally bound PRC1 is maternally provided

Next, we analyzed the onset of matPRC1 targeting. In fully grown germinal vesicle and metaphase-II oocytes, Rnf2, Bmi1, Cbx2 and Phc2 seemed not to be chromatin bound (**Fig. 3a** and **Supplementary Fig. 4** online; $n = 25–35$ per stage) although the maternal genome was trimethylated at H3K27 (**Supplementary Fig. 1**; $n = 10$ per stage). Shortly after gamete fusion, however, all four matPRC1 components rapidly accumulated at the maternal chromosomes that would constitute the embryo (arrow, **Fig. 3a**), whereas lower protein levels built up at chromosomes segregating into the second polar body. Concurrently, matPRC1 proteins were particularly enriched at DAPI-intense heterochromatin of paternal decondensing chromosomes (**Fig. 3b,c**).

We further asked whether matPRC1 proteins at paternal chromatin are transmitted through spermatozoa or maternally provided. We used a functional Rnf2 and yellow fluorescent protein (Rnf2–YFP) fusion knock-in allele (K.I. and H.K., unpublished data) to probe for YFP signal in heterozygous embryos. The Rnf2–YFP signal was only detectable after maternal transmission of the knock-in allele (**Fig. 4a**), indicating that most matPRC1 in zygotes is of maternal origin ($n = 10–15$ per genetic condition). Accordingly, using protein blot analysis, we found that Rnf2 protein levels increased upon gamete fusion (**Fig. 4b**), likely as a result of translational activation of maternal message.

Finally, we determined Rnf2 protein levels in mature mouse spermatozoa isolated from the caudal epididymus. By immunofluorescence, we did not detect any PRC1 signal in sperm (**Fig. 4c**). This was not a result of antibody inaccessibility, as we were able to detect chromatin markers, known to be present in mature sperm[8]. By protein blot analysis, we also failed to detect Rnf2 protein in spermatozoa, although we could detect the protein in low numbers of embryonic stem cells (**Fig. 4d**). These data support our finding that PRC1 in zygotes is primarily of maternal origin, although we cannot exclude the possibility that paternal proteins may seed binding of maternally provided PRC1.

### matPRC1 targeting to heterochromatin is *Ezh2* independent

At certain genes, PRC1 binding to chromatin depends on PRC2 function[27,28]. Therefore, we evaluated the role of PRC2 components in oocytes and early embryos. Like matPRC1 components (**Fig. 3a**), PRC2 components become enriched after gamete fusion at maternal chromosomes that will be retained in the embryo (**Fig. 5a** and **Supplementary Fig. 4**; $n = 25–30$ per stage). Protein blots showed increasing Ezh2 protein levels during oocyte meiosis and early embryogenesis (**Fig. 5b**), suggesting translational activation of maternal message. Nevertheless, in contrast to matPRC1 (**Fig. 3b**), PRC2

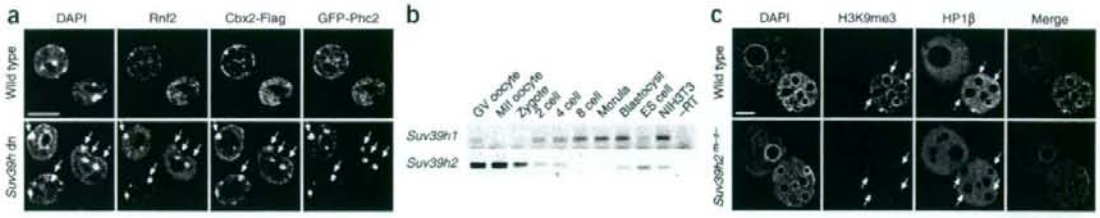


**Figure 7** Absence of H3K9me3 and HP1β allows matPRC1 targeting to constitutive heterochromatin in early embryos. (**a**) Immunofluorescence characterization of wild-type and *Suv39h* dn embryonic stem cells overexpressing three tagged matPRC1 components. Only in *Suv39h* dn embryonic stem cells, overexpressed Cbx2, Phc2 and Bmi1 (see **Supplementary Fig. 7**), as well as endogenous Rnf2 are retargeted to constitutive heterochromatin. Overexpressed Cbx2-Flag was detected using Cbx2-specific antibodies. For GFP-Phc2, the GFP signal was detected. (**b**) RT-PCR analysis of *Suv39h1* and *Suv39h2* on samples described in **Figure 1d** identifying Suv39h2 as the major maternal HMT and Suv39h1 as the main zygotic HMT. (**c**,**d**) Immunofluorescence staining of wild-type and *Suv39h2*$^{m-z-}$ zygotes. (**c**) H3K9me3 and HP1β are lost from maternal heterochromatin (arrows) in many *Suv39h2*$^{m-z-}$ embryos. HP1β is unaffected in euchromatin, despite reduction of underlying H3K9me3. (**d**) matPRC1 component Rnf2 localizes to maternal heterochromatin in absence of H3K9me3 and HP1β (arrow). Scale bars, 10 μm.

members ($n$ = 27) or H3K27me3 ($n$ = 22) did not label paternal chromatin shortly after gamete fusion (**Fig. 5c** and **Supplementary Fig. 1**), suggesting that initial targeting of matPRC1 to paternal heterochromatin is PRC2 independent.

To unequivocally determine the role of PRC2 in matPRC1 targeting to paternal heterochromatin, we used a conditional deficiency allele for *Ezh2* in which exons 16 and 17, containing parts of the catalytic SET domain, are flanked by loxP sites (**Supplementary Fig. 5** online; X.M. and S.H.O., unpublished data). Loss of *Ezh2* function using this allele leads to gastrulation defects and post-implantation embryonic lethality (**Supplementary Fig. 5**), as described for a conventional deletion allele[33]. We subsequently bred in *Zp3*-cre and *Prm1*-cre transgenic lines that mediate gene deletion in primary oocytes and elongating spermatids, respectively, in order to generate embryos that were deficient for maternal and zygotic *Ezh2* expression (*Ezh2*$^{m-z-}$) (**Supplementary Fig. 5**), and that lacked detectable Ezh2 protein (**Fig. 5d**; $n$ = 35). We did not detect *de novo* H3K27me2/3 in late-stage paternal pronuclei (**Fig. 5e**; $n$ = 75). In maternal pre-replication pronuclei, H3K27me2/3 levels were similar in wild type and *Ezh2*$^{m-z-}$ zygotes, indicating that after *Zp3*-cre–mediated Ezh2 depletion, previously established H3K27me2/3 remains stably present in maturing oocytes. After replication, however, H3K27me2/3 levels were strongly reduced in maternal pronuclei (**Fig. 5e**). H3K27me3 was undetectable from late 2-cell to blastocyst stage (data not shown), indicating that Ezh2 is required for the establishment and maintenance of global H3K27me3 at both parental genomes. H3K27me1 is, however, independent of Ezh2 (**Fig. 5e**; $n$ = 10).

Through double-labeling experiments, we found that in zygotes targeting of all four matPRC1 components to euchromatin correlated with levels of H3K27me3 labeling. MatPRC1 staining was undetectable on paternal euchromatin, whereas it was severely reduced on maternal euchromatin (**Fig. 5f** and **Supplementary Fig. 6** online; wild type, $n$ = 43; *Ezh2*$^{m-z-}$, $n$ = 42). In contrast, matPRC1 remained enriched at paternal constitutive heterochromatin in *Ezh2*$^{m-z-}$ embryos up to the 8-cell stage (**Fig. 5f** and **Supplementary Fig. 6**; data not shown), indicating PRC2-independent targeting of matPRC1 to paternal constitutive heterochromatin.

### Parental-specific marking of cleavage chromosomes

We subsequently studied the mechanism of mitotic transmission. Unlike HP1β, which dissociated from mitotic chromosomes (**Fig. 5g**)[34], Rnf2 remained bound along metaphase chromosomes in a banded pattern ($n$ = 10). For higher-resolution analyses, we studied prometaphase chromosomes of embryos at successive cleavage stages (**Fig. 6a**). At the first cleavage division, Rnf2 was strongly enriched at the proximal DAPI-intense heterochromatic chromosome ends of paternal origin but not at maternal chromosome ends, which were enriched in H3K9me3. At the second and third divisions, Rnf2 labeling of paternal pericentric heterochromatin was moderately and strongly reduced, respectively (relative to euchromatin; see below). In contrast, pericentric heterochromatin of maternal chromosomes was moderately labeled by H3K9me3 during the first three cleavages. At the fourth division, all chromosomes ends were highly enriched in H3K9me3, indicating acquisition and consolidation of the canonical *Suv39h*-mediated identity at paternal and maternal heterochromatin, respectively, during the 8-cell stage. In summary, these analyses demonstrate mitotically stable but transient marking of paternal heterochromatin by matPRC1 components (**Fig. 6b**).

In addition to asymmetric heterochromatic labeling, we also observed differential marking along chromosome arms over the first three cleavage divisions (**Fig. 6**). Rnf2 showed clear banding patterns along paternal chromosomes that were much less pronounced along maternal chromosomes. Conversely, the maternal complement was more strongly marked by H3K9me3 banding patterns. This dual asymmetry was lost at the fourth cleavage.

### *Suv39h*-pathway impairs PRC1 targeting to heterochromatin

We next addressed the mechanism of parental-specific matPRC1 targeting. We reasoned that matPRC1 targeting to paternal constitutive heterochromatin could be due to a chromatin configuration inherited from sperm[4,8] and/or the absence of a functional *Suv39h* pathway. Intrigued by the mutually exclusive labeling by matPRC1 versus H3K9me3 (**Figs. 2** and **6**), we first analyzed *Suv39h1* and *Suv39h2* double null (*Suv39h* dn) embryonic stem cells that harbor H3K27me3 at constitutive heterochromatin in the absence of H3K9me3 (ref. 31; **Supplementary Fig. 7** online). Nonetheless, we

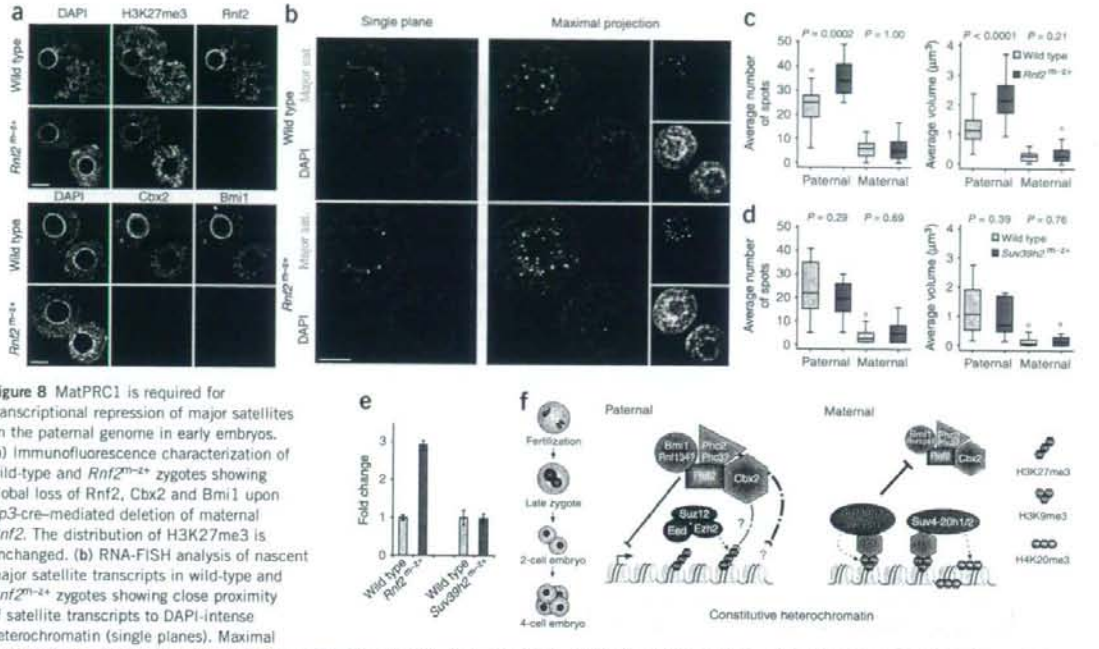


**Figure 8** MatPRC1 is required for transcriptional repression of major satellites on the paternal genome in early embryos. (**a**) Immunofluorescence characterization of wild-type and $Rnf2^{m-z+}$ zygotes showing global loss of Rnf2, Cbx2 and Bmi1 upon *Zp3*-cre–mediated deletion of maternal *Rnf2*. The distribution of H3K27me3 is unchanged. (**b**) RNA-FISH analysis of nascent major satellite transcripts in wild-type and $Rnf2^{m-z+}$ zygotes showing close proximity of satellite transcripts to DAPI-intense heterochromatin (single planes). Maximal projections visualize total number of transcription sites per pronucleus. Scale bars, 10 μm. (**c**) Average number and volume of major satellite transcription sites for wild-type ($n = 20$) and $Rnf2^{m-z+}$ ($n = 25$) pronuclei represented as boxplots (see Methods). In $Rnf2^{m-z+}$ zygotes, the number and volume of transcription sites are significantly increased in paternal but not maternal pronuclei compared to wild-type embryos. *P* values were calculated using a paired *t*-test. (**d**) Average number and volume of major satellite transcription sites for wild-type ($n = 28$) and $Suv39h2^{m-z+}$ ($n = 10$) pronuclei represented as boxplots. Major satellite levels remain unchanged in maternal pronuclei of $Suv39h2^{m-z+}$ zygotes. (**e**) Quantitative RT-PCR analysis of major satellite transcription in late 2-cell embryos showing a threefold increased transcript level in $Rnf2^{m-z+}$ versus wild-type embryos, whereas levels remain unaltered in *Suv39h2* maternal mutants compared to wild-type controls. Error bars represent s.d. of three PCR amplifications for each sample. Similar results were obtained in two independent experiments. (**f**) Model for the establishment of distinct chromatin states at constitutive heterochromatin in the early embryo by Suv39h and PRC1 pathways in a parent of origin–dependent manner.

failed to detect heterochromatic enrichment for Rnf2, Phc1 or Mel18 (**Supplementary Fig. 7**), expressed in embryonic stem cells (**Fig. 1d**)[35]. Likewise, we failed to detect PRC1 members at constitutive heterochromatin in quiescent B cells (data not shown), devoid of *Suv39h*-mediated repressive modifications[36]. To test whether lack of detection was a result of low expression levels of one or more matPRC1 components, we reconstituted matPRC1 by co-overexpressing Cbx2-Flag, GFP-Phc2 and 3Flag-Bmi1 in wild-type and *Suv39h* dn embryonic stem cells and analyzed their nuclear localization (**Fig. 7a** and **Supplementary Fig. 7**). All overexpressed PRC1 components as well as endogenously expressed Rnf2 were targeted to constitutive heterochromatin in *Suv39h* dn embryonic stem cells but not in wild-type cells. These data show that PRC1 enrichment at heterochromatin is not unique to early embryos, excluding the necessity of a 'paternal imprint' for targeting, and that the *Suv39h* pathway blocks matPRC1 loading to heterochromatin.

We subsequently investigated the interplay between *Suv39h* and matPRC1 *in vivo*. As most *Suv39h* dn mice die during late gestation or are postnatally growth retarded[13], we studied whether maternal deficiency for Suv39h2, the enzyme predominantly expressed in oocytes (**Fig. 7b**), creates a hypomorphic condition in zygotic embryos. Indeed, in 71% ($n = 34$) of maternally (and zygotically) deficient *Suv39h2* zygotes, maternal heterochromatic labeling of H3K9me3 and HP1β was lost, although euchromatic HP1β labeling was unaffected (**Fig. 7c**). In such embryos, we observed strong enrichment for matPRC1 components at maternal heterochromatin and thus alleviation of parent of origin–specific labeling (**Fig. 7d** and **Supplementary Fig. 7**). Through analysis of wild-type and $Suv39h2^{m-z-}$ embryos, we found a highly significant inverse correlation between levels of H3K9me3 and HP1β versus those of matPRC1 components at constitutive heterochromatin ($P = 8.47 \times 10^{-10}$; $n = 103$; Fisher's exact test for dependency). These data unequivocally demonstrate that paternal heterochromatic enrichment of matPRC1 is due to the lack of local Suv39h activity instead of germline transmission of a paternal-specific factor or chromatin state.

### MatPRC1 represses major satellites in early embryos

Finally, we generated embryos lacking matPRC1 to determine the functional significance of matPRC1 for transcriptional repression. We used a conditional deficiency allele for *Rnf2* in which major parts of the Ring finger domain were flanked by loxP sites (E.B. and M.v.L., unpublished data). The same targeting strategy was used to generate a conventional deletion allele that causes gastrulation defects in $Rnf2^{-/-}$ mice[37]. We crossed conditional *Rnf2* mice with a *Zp3*-cre transgenic line to generate embryos that were maternally deficient for *Rnf2* and that lacked detectable Rnf2 protein in zygotes (**Fig. 8a**). H3K27me3

distribution was unchanged in *Rnf2*$^{m-z+}$ zygotes (**Fig. 8a**). In contrast, Cbx2 and Bmi1 were undetectable (**Fig. 8a**), indicating that Rnf2 is required for the stability of matPRC1, as observed in *Rnf2*$^{-/-}$ embryonic stem cells[35]. To measure nascent transcript levels of major satellites[38], we carried out RNA-FISH in zygotes (**Fig. 8b**). We observed foci adjacent to DAPI-intense heterochromatin. As detection of foci was sensitive to treatment with the transcription elongation inhibitor DRB (data not shown), our results show *de novo* transcription in one-cell embryos, before genome-wide activation at the 2-cell stage. In wild-type zygotes, major satellite transcript levels were fivefold higher in paternal versus maternal pronuclei (**Fig. 8c**), consistent with the higher transcriptional potential of the paternal pronucleus[39]. Major satellite transcription was unchanged in maternal pronuclei of wild-type versus *Rnf2*$^{m-z+}$ zygotes, correlating with the local presence of *Suv39h*-mediated repressive chromatin marks. In paternal pronuclei of *Rnf2*$^{m-z+}$ zygotes, however, the number of major satellite transcription sites and the total level of nascent transcripts were significantly increased compared to wild-type paternal pronuclei (**Fig. 8c**). Consistently, in *Rnf2*$^{m-z+}$ 2-cell embryos, major satellites were threefold upregulated (**Fig. 8e**). Thus, these data unambiguously demonstrate that matPRC1 is required for transcriptional repression of underlying major satellites.

As reported before[18], we measured a fourfold upregulation of major satellite expression in *Suv39h* dn embryonic stem cells over wild-type controls (**Supplementary Fig. 7**). Through RNA-FISH analysis of *Suv39h2*$^{m-z+}$ zygotes, however, we found no significant increase in major satellite transcript levels in maternal pronuclei despite the lack of H3K9me3 and HP1β at pericentric heterochromatin (**Fig. 8d**). Similarly, we observed no change in transcript levels in *Suv39h2*$^{m-z+}$ 2-cell embryos (**Fig. 8e**). These results strongly suggest that matPRC1 recruited to maternal constitutive heterochromatin in *Suv39h2* mutant early embryos functions as a repressive back-up mechanism.

## DISCUSSION

Parent of origin–dependent differential marking by active and repressive epigenetic modifications is reminiscent of allelic specification underlying imprinted X inactivation and genomic imprinting. Here we show that two repressive pathways specify the 'allelic' states of maternal and paternal constitutive heterochromatin, suggesting functional compensation. Maternally, pericentric heterochromatin is marked by H3K9me3 and H4K20me3, two modifications established by the Suv39h and Suv4-20h HMTs in oocytes, and by HP1β loaded onto chromatin upon gamete fusion. In contrast, maternally provided PRC1 complexes that are required for transcriptional repression of underlying major satellites associate with paternal heterochromatin during sperm nuclear decondensation. Deficiency for *Suv39h2* results in targeting of matPRC1 to maternal heterochromatin only when it is devoid of detectable H3K9me3 and/or HP1β. Absence of paternal germ-line derived H3K9me3 therefore serves as the primary germ-line imprint for targeting matPRC1 to major satellites of the paternal genome (**Fig. 8f**). Consistently, major satellite expression was not upregulated in *Suv39h2*$^{m-z+}$ early embryos but was upregulated in *Suv39h* dn embryonic stem cells lacking heterochromatic PRC1. In absence of H3K9me3, PRC1 thus constitutes the default repressive pathway for constitutive heterochromatin formation in early embryos. The identity of maternal heterochromatin is inherited from the oocyte, assigning a crucial role to *Suv39h*-mediated H3K9me3 in *trans*-generational inheritance of maternal epigenetic states in mouse and likely other mammals.

The fact that a matPRC1-like complex, when overexpressed, is targeted to heterochromatin of *Suv39h* dn embryonic stem cells underscores the absence of a 'selective paternal imprint' needed for heterochromatic association. This result confirms the dominant role of the *Suv39h* pathway in blocking matPRC1 binding to heterochromatin and emphasizes the dosage sensitivity of matPRC1 association to chromatin. Notably, absence of H3K9me3 correlates with H3K27me3 enrichment at pericentric heterochromatin in wild-type early embryos and *Suv39h* dn embryonic stem cells, indicating that Suv39h is also dominant over PRC2.

Given the dominance of Suv39h in defining heterochromatin, it is of note that the paternal genome is initially refractory toward *de novo* H3K9 trimethylation. It is possible that the maternal Suv39h2 protein, if present, is enzymatically inhibited, as reported for a H3K9 dimethyltransferase[5], or its activity is locally counteracted by a histone demethylase. In analogy to heterochromatin maturation in fly embryos[40] or *Schizosaccharomyces pombe*[17], conditions that enable '*de novo*' targeting of Suv39h enzymes may first need to be established in mammalian embryos.

In mature quiescent oocytes, PcG proteins are not detectable at chromatin, although they are expressed. Only after germ cell fusion do they associate to maternal anaphase II chromosomes. These dynamics are reminiscent of those of other transcription and chromatin factors in quiescent oocytes[41] and M-II oocytes[42], and may facilitate the transition of the maternal-to-zygotic transcription program. At the paternal genome, matPRC1 is loaded onto heterochromatin during sperm decondensation, before repressive histone methylation marks are acquired. Consistently, Ezh2-mediated H3K27me3 is not required for matPRC1 targeting to paternal heterochromatin. This shows that despite the binding affinity of Cbx2 toward H3K27me3[27], the interaction between Cbx2 and H3K27me3 is not the sole mechanism for chromatin targeting of matPRC1. In analogy to X inactivation[23,43], genomic imprinting[44] and constitutive heterochromatin formation in somatic cells[45], a noncoding RNA may be required for matPRC1 heterochromatic localization. Alternatively, matPRC1 recruitment may depend on the repetitive nature and/or AT-richness of the underlying sequences.

The kinetics of H3K9me3 and matPRC1 chromatin association suggest two phases of epigenetic programming during preimplantation development. The first phase, lasting until the 8-cell stage, is characterized by parental asymmetry in histone modifications[7,9], DNA methylation[3] and PcG proteins. Besides pericentric regions, paternal and maternal mitotic chromosome arms are also differentially labeled by matPRC1 and H3K9me3, respectively. Given the requirement of matPRC1 for transcriptional repression of major satellites, matPRC1 likely represses other sequences in the paternal genome, whereas H3K9me3 could contribute to repression in the maternal genome. The *Suv39h2* loss-of-function study demonstrates that epigenetic programming is flexible in the early embryo, being adaptable to variable chromatin states established during preceding oogenesis (**Fig. 7**) and likely spermatogenesis[46]. This plasticity may facilitate the maternal-to-zygotic transition in gene expression at both genomes as well as the reacquisition of totipotency.

The resolution of parental epigenetic asymmetry during the 8-cell stage marks the onset of the second phase of epigenetic programming. Besides a possible gain in *Suv39h1* function, the change in paternal repressive identity is probably supported by reduced expression of certain matPRC1 components. Accordingly, we did not detect Phc2, and we found that Cbx2 was strongly downregulated in 16-cell and later stage embryos (**Supplementary Fig. 2**). Of note, the resolution of epigenetic asymmetry coincides with a number of key developmental changes characteristic of the 8-cell stage that reflect preparation for the successive cell determination decisions. For example, blastomeres start

to compact and polarize, leading to the formation of precursors of the embryonic and extra-embryonic cell lineages[47]. Concurrently, active histone modifications start to be removed from the paternal X chromosome undergoing imprinted inactivation[48]. We observed Rnf2 accumulation at the presumptive Xi domain from the 16-cell stage onwards, thus directly after Rnf2 displacement from constitutive heterochromatin. On the basis of the overall kinetics, it is likely that resolution of global parental epigenetic asymmetry is needed to enable subsequent specification of cellular lineages.

In conclusion, our analyses establish the concept of epigenetic asymmetry between parental genomes during preimplantation development as a dynamic response to differential maturation of chromatin states during oogenesis versus spermatogenesis. We anticipate that PRC1 has a role in epigenetic gene regulation during preimplantation development[49].

## METHODS

**Mice and cell lines.** To produce maternally deficient *Ezh2* oocytes, we generated $Ezh2^{F/F}$ mice that carried the *Zp3*-cre (zona pellucida3–cre) recombinase transgene, mediating efficient deletion in dictyate-stage growing primary oocytes. In addition, we used a *Prm1*-cre (protamine1-cre) line, which expresses Cre recombinase during late spermatogenesis, to generate sperm carrying the mutant *Ezh2* allele. Maternal and paternal *Ezh2*-deficient embryos were obtained from matings between $Ezh2^{F/F}$; *Zp3*-cre/+ females and $Ezh2^{F/F}$; *Prm1*-cre/+ males. Control embryos designated as wild-type were $Ezh2^{F/F}$. Maternally deficient *Rnf2* zygotes were generated by crossing $Rnf2^{F/F}$; *Zp3*-cre/+ females with $Rnf2^{F/F}$ males. Wild-type control embryos were generated by $Rnf2^{F/F}$, $Rnf2^{F/+}$ or $Rnf2^{F/-}$ females and $Rnf2^{F/F}$ males. The generation of *Suv39h2* mutant mice has been described previously[13]. Wild-type control embryos were generated by $Suv39h2^{+/-}$ females and $Suv39h2^{+/+}$ males. Embryos polymorphic for pericentromeric heterochromatin were obtained from matings of C57BL6 females with JF1 males. For further information on mouse lines, embryo isolation and description of cell lines, see **Supplementary Methods** online. Housing and handling of mice conformed to the Swiss Animal Protection Ordinance, chapter 1.

**Immunofluorescence and FISH.** Immunofluorescence[7] and FISH[48] of embryos were carried out as previously described, with some modifications described in the **Supplementary Methods**.

**Microscopy and image analysis.** Immunofluorescence stainings of embryonic stem cells and embryos were analyzed using a laser scanning confocal microscope LSM510 META (Zeiss) and LSM510 software. For embryos, we recorded a *z* series of either 0.3 μm or 0.5-μm slices or scanned one confocal slice through the maximal radius of each (pro)nucleus; we then exported the slices as 8-bit TIFF files, later projected using Photoshop 9.0. For numerical evaluation, all images of embryos taken for a given modification were analyzed individually and scored as follows: (–) no staining; (=) equal staining at hetero- and euchromatin; (>) enhanced and (≫) strongly enhanced staining at heterochromatin versus euchromatin. Cleavage-stage embryos were scanned in three dimensions, recording a *z* series of 0.5-μm slices. Only long prometaphase chromosomes were evaluated for scoring heterochromatin labeling and banding patterns along chromosome arms. Embryos processed by Immuno-FISH were analyzed with a spinning disk confocal microscope (Yokogawa CSU-22). For RNA-FISH analysis of major satellite expression in zygotes, a *z* series of 0.3 μm was recorded for each zygote using the confocal microscope LSM510 META (Zeiss). The number of major satellite transcription sites and the volume of each spot were calculated for paternal and maternal pronuclei using 3D Spotfinder software in Imaris 5.9.0. alpha. Sites of major satellite transcription with a minimum volume of 0.01 $\mu m^3$ were identified, and the volume of each spot was summed up to represent the total volume of major satellite transcription per pronucleus.

**Statistical analysis.** We investigated a possible functional association between PRC1 and HP1β using wild-type ($n = 69$) and *Suv39h2* maternally and zygotically deficient embryos ($n = 34$). For each embryo, PRC1 and HP1 complexes were stained and classified according to staining intensity into four categories. We summarized the data in a four-by-four contingency table and tested the significance of the association between PRC1 and HP1 using Fisher's exact test.

Results of major satellite transcription levels measured by RNA-FISH are presented as boxplots with the thick line representing the median, the top and bottom boundaries of the boxes corresponding to the 75 and 25 percentiles, respectively, and the top and bottom whiskers presenting maximum and minimum values, respectively. Values that deviate more than the 1.5-fold distance between quartiles from the median are drawn as black circles and represent outliers. *P* values were calculated using a paired *t*-test.

**RT-PCR and protein blot.** Gene expression analysis of oocytes and embryos was carried out as described in the **Supplementary Methods**. Protein blot analysis was carried out using standard procedures. Preparation of oocytes, embryos and sperm samples for protein blot analysis is described in the **Supplementary Methods**.

*Note: Supplementary information is available on the Nature Genetics website.*


### ACKNOWLEDGMENTS

We thank M. Vidal (Centro de Investigaciones Biológicas, Spain) and T. Jenuwein (Research Institute of Molecular Pathology, Austria) for providing antisera. Moreover, we are grateful to T. Jenuwein and B. Knowles (The Jackson Laboratory, USA) for providing *Suv39h2* deficient and *Zp3*-cre transgenic mice, respectively. We acknowledge excellent assistance by Friedrich Miescher Institute (FMI) colleagues P. Schwarb and J. Rietdorf (microscopy and imaging facility), B. Heller-Stilb and J.-F. Spetz (animal facility), S. Bichet (histology) and M. Stadler (bioinformatics). We thank members of the Peters laboratory for fruitful discussions and P. de Boer, D. Schübeler, S. Gasser and P. Hublitz for valuable comments on the manuscript. Research at the Friedrich Miescher Institute is supported by the Novartis Research Foundation. M.P. acknowledges the Boehringer Ingelheim Fonds for her PhD fellowship. Research in the Peters laboratory is supported by the EU NoE network 'The Epigenome' (LSHG-CT-2004-503433).


### AUTHOR CONTRIBUTIONS

M.P. and A.H.F.M.P. conceived and designed the experiments. M.P., R.T., U.B. and C.K. performed the experiments. M.P., R.T., U.B. and A.H.F.M.P. analyzed the data. A.P.O. provided antibodies. E.B. and M.v.L. provided conditionally deficient *Rnf2* mice. X.M. and S.H.O. provided conditionally deficient *Ezh2* mice. K.I. and H.K. provided *Rnf2*–YFP knock-in mice. M.P. and A.H.F.M.P. wrote the manuscript.


Published online at http://www.nature.com/naturegenetics
Reprints and permissions information is available online at http://npg.nature.com/reprintsandpermissions



1. Surani, M.A., Hayashi, K. & Hajkova, P. Genetic and epigenetic regulators of pluripotency. *Cell* **128**, 747–762 (2007).
2. Arney, K.L., Bao, S., Bannister, A.J., Kouzarides, T. & Surani, M.A. Histone methylation defines epigenetic asymmetry in the mouse zygote. *Int. J. Dev. Biol.* **46**, 317–320 (2002).
3. Dean, W. *et al.* Conservation of methylation reprogramming in mammalian development: aberrant reprogramming in cloned embryos. *Proc. Natl. Acad. Sci. USA* **98**, 13734–13738 (2001).
4. Govin, J. *et al.* Pericentric heterochromatin reprogramming by new histone variants during mouse spermiogenesis. *J. Cell Biol.* **176**, 283–294 (2007).
5. Liu, H., Kim, J.M. & Aoki, F. Regulation of histone H3 lysine 9 methylation in oocytes and early pre-implantation embryos. *Development* **131**, 2269–2280 (2004).
6. Martin, C. *et al.* Genome restructuring in mouse embryos during reprogramming and early development. *Dev. Biol.* **292**, 317–332 (2006).
7. Santos, F., Peters, A.H., Otte, A.P., Reik, W. & Dean, W. Dynamic chromatin modifications characterise the first cell cycle in mouse embryos. *Dev. Biol.* **280**, 225–236 (2005).
8. van der Heijden, G.W. *et al.* Transmission of modified nucleosomes from the mouse male germline to the zygote and subsequent remodeling of paternal chromatin. *Dev. Biol.* **298**, 458–469 (2006).
9. van der Heijden, G.W. *et al.* Asymmetry in histone H3 variants and lysine methylation between paternal and maternal chromatin of the early mouse zygote. *Mech. Dev.* **122**, 1008–1022 (2005).
10. Merico, V. *et al.* Epigenomic differentiation in mouse preimplantation nuclei of biparental, parthenote and cloned embryos. *Chromosome Res.* **15**, 341–360 (2007).

11. Kishigami, S. *et al.* Epigenetic abnormalities of the mouse paternal zygotic genome associated with microinsemination of round spermatids. *Dev. Biol.* **289**, 195–205 (2006).
12. Ekwall, K. *et al.* Mutations in the fission yeast silencing factors clr4+ and rik1+ disrupt the localisation of the chromo domain protein Swi6p and impair centromere function. *J. Cell Sci.* **109**, 2637–2648 (1996).
13. Peters, A.H. *et al.* Loss of the Suv39h histone methyltransferases impairs mammalian heterochromatin and genome stability. *Cell* **107**, 323–337 (2001).
14. Peters, A.H. & Schubeler, D. Methylation of histones: playing memory with DNA. *Curr. Opin. Cell Biol.* **17**, 230–238 (2005).
15. Wustmann, G., Szidonya, J., Taubert, H. & Reuter, G. The genetics of position-effect variegation modifying loci in *Drosophila melanogaster*. *Mol. Gen. Genet.* **217**, 520–527 (1989).
16. Lachner, M., O'Carroll, D., Rea, S., Mechtler, K. & Jenuwein, T. Methylation of histone H3 lysine 9 creates a binding site for HP1 proteins. *Nature* **410**, 116–120 (2001).
17. Grewal, S.I. & Jia, S. Heterochromatin revisited. *Nat. Rev. Genet.* **8**, 35–46 (2007).
18. Lehnertz, B. *et al.* Suv39h-mediated histone H3 lysine 9 methylation directs DNA methylation to major satellite repeats at pericentric heterochromatin. *Curr. Biol.* **13**, 1192–1200 (2003).
19. Schotta, G. *et al.* A silencing pathway to induce H3–K9 and H4–K20 trimethylation at constitutive heterochromatin. *Genes Dev.* **18**, 1251–1262 (2004).
20. Ringrose, L. & Paro, R. Epigenetic regulation of cellular memory by the Polycomb and Trithorax group proteins. *Annu. Rev. Genet.* **38**, 413–443 (2004).
21. Schwartz, Y.B. & Pirrotta, V. Polycomb silencing mechanisms and the management of genomic programmes. *Nat. Rev. Genet.* **8**, 9–22 (2007).
22. Levine, S.S., King, I.F. & Kingston, R.E. Division of labor in polycomb group repression. *Trends Biochem. Sci.* **29**, 478–485 (2004).
23. de Napoles, M. *et al.* Polycomb group proteins Ring1A/B link ubiquitylation of histone H2A to heritable gene silencing and X inactivation. *Dev. Cell* **7**, 663–676 (2004).
24. Wang, H. *et al.* Role of histone H2A ubiquitination in Polycomb silencing. *Nature* **431**, 873–878 (2004).
25. Sparmann, A. & van Lohuizen, M. Polycomb silencers control cell fate, development and cancer. *Nat. Rev. Cancer* **6**, 846–856 (2006).
26. Boyer, L.A. *et al.* Polycomb complexes repress developmental regulators in murine embryonic stem cells. *Nature* **441**, 349–353 (2006).
27. Bernstein, E. *et al.* Mouse polycomb proteins bind differentially to methylated histone H3 and RNA and are enriched in facultative heterochromatin. *Mol. Cell. Biol.* **26**, 2560–2569 (2006).
28. Fujimura, Y. *et al.* Distinct roles of Polycomb group gene products in transcriptionally repressed and active domains of Hoxb8. *Development* **133**, 2371–2381 (2006).
29. Guenatri, M., Bailly, D., Maison, C. & Almouzni, G. Mouse centric and pericentric satellite repeats form distinct functional heterochromatin. *J. Cell Biol.* **166**, 493–505 (2004).
30. Probst, A.V., Santos, F., Reik, W., Almouzni, G. & Dean, W. Structural differences in centromeric heterochromatin are spatially reconciled on fertilisation in the mouse zygote. *Chromosoma* **116**, 403–415 (2007).
31. Peters, A.H. *et al.* Partitioning and plasticity of repressive histone methylation states in mammalian chromatin. *Mol. Cell* **12**, 1577–1589 (2003).
32. Mayer, W., Smith, A., Fundele, R. & Haaf, T. Spatial separation of parental genomes in preimplantation mouse embryos. *J. Cell Biol.* **148**, 629–634 (2000).
33. O'Carroll, D. *et al.* The polycomb-group gene Ezh2 is required for early mouse development. *Mol. Cell. Biol.* **21**, 4330–4336 (2001).
34. Fischle, W. *et al.* Regulation of HP1-chromatin binding by histone H3 methylation and phosphorylation. *Nature* **438**, 1116–1122 (2005).
35. Leeb, M. & Wutz, A. Ring1B is crucial for the regulation of developmental control genes and PRC1 proteins but not X inactivation in embryonic cells. *J. Cell Biol.* **178**, 219–229 (2007).
36. Baxter, J. *et al.* Histone hypomethylation is an indicator of epigenetic plasticity in quiescent lymphocytes. *EMBO J.* **23**, 4462–4472 (2004).
37. Voncken, J.W. *et al.* Rnf2 (Ring1b) deficiency causes gastrulation arrest and cell cycle inhibition. *Proc. Natl. Acad. Sci. USA* **100**, 2468–2473 (2003).
38. Lu, J. & Gilbert, D.M. Proliferation-dependent and cell cycle regulated transcription of mouse pericentric heterochromatin. *J. Cell Biol.* **179**, 411–421 (2007).
39. Aoki, F., Worrad, D.M. & Schultz, R.M. Regulation of transcriptional activity during the first and second cell cycles in the preimplantation mouse embryo. *Dev. Biol.* **181**, 296–307 (1997).
40. Rudolph, T. *et al.* Heterochromatin formation in *Drosophila* is initiated through active removal of H3K4 methylation by the LSD1 homolog SU(VAR)3–3. *Mol. Cell* **26**, 103–115 (2007).
41. Sun, F. *et al.* Nuclear reprogramming: the zygotic transcription program is established through an "erase-and-rebuild" strategy. *Cell Res.* **17**, 117–134 (2007).
42. Yoshida, N., Brahmajosyula, M., Shoji, S., Amanai, M. & Perry, A.C. Epigenetic discrimination by mouse metaphase II oocytes mediates asymmetric chromatin remodeling independently of meiotic exit. *Dev. Biol.* **301**, 464–477 (2007).
43. Schoeftner, S. *et al.* Recruitment of PRC1 function at the initiation of X inactivation independent of PRC2 and silencing. *EMBO J.* **25**, 3110–3122 (2006).
44. Umlauf, D. *et al.* Imprinting along the Kcnq1 domain on mouse chromosome 7 involves repressive histone methylation and recruitment of Polycomb group complexes. *Nat. Genet.* **36**, 1296–1300 (2004).
45. Maison, C. *et al.* Higher-order structure in pericentric heterochromatin involves a distinct pattern of histone modification and an RNA component. *Nat. Genet.* **30**, 329–334 (2002).
46. Chong, S. *et al.* Modifiers of epigenetic reprogramming show paternal effects in the mouse. *Nat. Genet.* **39**, 614–622 (2007).
47. Johnson, M.H. Manipulation of early mammalian development: what does it tell us about cell lineages? *Dev Biol (N Y 1985)* **4**, 279–96 (1986).
48. Okamoto, I., Otte, A.P., Allis, C.D., Reinberg, D. & Heard, E. Epigenetic dynamics of imprinted X inactivation during early mouse development. *Science* **303**, 644–649 (2004).
49. Blewitt, M.E., Vickaryous, N.K., Paldi, A., Koseki, H. & Whitelaw, E. Dynamic reprogramming of DNA methylation at an epigenetically sensitive allele in mice. *PLoS Genet.* **2**, e49 (2006).

Development 135, 1513-1524 (2008) doi:10.1242/dev.014340

# Polycomb group proteins Ring1A/B are functionally linked to the core transcriptional regulatory circuitry to maintain ES cell identity

**Mitsuhiro Endoh[1], Takaho A. Endo[2], Tamie Endoh[1], Yu-ichi Fujimura[1], Osamu Ohara[1], Tetsuro Toyoda[2], Arie P. Otte[3], Masaki Okano[4], Neil Brockdorff[5], Miguel Vidal[1,6] and Haruhiko Koseki[1,*]**

The Polycomb group (PcG) proteins mediate heritable silencing of developmental regulators in metazoans, participating in one of two distinct multimeric protein complexes, the Polycomb repressive complexes 1 (PRC1) and 2 (PRC2). Although PRC2 has been shown to share target genes with the core transcription network, including Oct3/4, to maintain embryonic stem (ES) cells, it is still unclear whether PcG proteins and the core transcription network are functionally linked. Here, we identify an essential role for the core PRC1 components Ring1A/B in repressing developmental regulators in mouse ES cells and, thereby, in maintaining ES cell identity. A significant proportion of the PRC1 target genes are also repressed by Oct3/4. We demonstrate that engagement of PRC1 at target genes is Oct3/4-dependent, whereas engagement of Oct3/4 is PRC1-independent. Moreover, upon differentiation induced by Gata6 expression, most of the Ring1A/B target genes are derepressed and the binding of Ring1A/B to their target loci is also decreased. Collectively, these results indicate that Ring1A/B-mediated Polycomb silencing functions downstream of the core transcriptional regulatory circuitry to maintain ES cell identity.

**KEY WORDS: Polycomb, Oct3/4 (Pou5f1), Gata6, ES cells, Chromatin, Silencing, Ring1A/B (Ring1/Rnf2), Mouse**

## INTRODUCTION

Embryonic stem (ES) cells derived from the inner cell mass (ICM) of mammalian blastocyst-stage embryos have unlimited growth potential while maintaining pluripotency – the ability to differentiate into all tissue types except the placenta (Evans and Kaufman, 1981; Martin, 1981). These properties of ES cells are maintained by symmetrical self-renewal, producing two identical stem cell daughters upon cell division (Burdon et al., 2002). The maintenance of ES cell pluripotency is thought to involve a transcriptional regulatory hierarchy including the transcription factors Oct3/4 (Pou5f1 – Mouse Genome Informatics), Sox2 and Nanog, which may be central components judging by their unique expression patterns and essential roles during early murine development (Avilion et al., 2003; Chambers et al., 2003; Mitsui et al., 2003; Nichols et al., 1998).

Recent genome-wide chromatin immunoprecipitation (ChIP) analyses revealed that OCT4, SOX2 and NANOG co-occupy the promoters of a large group of genes in human ES cells (Boyer et al., 2005), suggesting that these factors form a core regulatory feedback circuit, in which all three factors regulate the expression of themselves as well as of each other (Catena et al., 2004; Kuroda et al., 2005; Okumura-Nakanishi et al., 2005; Rodda et al., 2005). This positive-feedback loop promotes self-renewal of pluripotent ES cells by repressing transcription factors involved in differentiation and development, whilst likely activating the expression of genes involved in ES cell maintenance (Boyer et al., 2005).

The execution of differentiation programs in ES cells is likely to be preceded by interruption of the positive-feedback loop by developmental regulators such as Cdx2 and Gata6. The expression of Cdx2 and Gata6 is repressed by Oct3/4 and Nanog in undifferentiated ES cells (Boyer et al., 2005; Loh et al., 2006; Mitsui et al., 2003; Niwa et al., 2000; Niwa et al., 2005), and the enforced expression of Cdx2 and Gata6 quickly shuts down the positive loop and promotes a rapid transition from the undifferentiated to the differentiated state (Fujikura et al., 2002; Niwa et al., 2005). Therefore, the positive-feedback loops and developmental regulators are reciprocally engaged to maintain ES cell identity; however, the molecular mechanisms underlying this reciprocal interaction are not fully understood.

The Polycomb group (PcG) of proteins mediate heritable silencing of developmental regulators in metazoans, participating in one of two distinct multimeric protein complexes, the Polycomb repressive complexes 1 (PRC1) and 2 (PRC2) (Cao et al., 2002; Czermin et al., 2002; Kuzmichev et al., 2002; Muller et al., 2002; Shao et al., 1999). In mammals, the core PRC2 is composed of Eed, Ezh2 and Suz12 and catalyses trimethylation of histone H3 at lysine 27 (H3K27), which in turn is thought to provide a recruitment site for PRC1 (Cao et al., 2002; Czermin et al., 2002; Fischle et al., 2003; Kuzmichev et al., 2002; Min et al., 2003). The core PRC1 is composed of orthologs of *Drosophila* Polycomb (Cbx2, Cbx4 and Cbx8), Posterior sex combs [Mel18 (Pcgf2) and Bmi1], Sex comb extra (Ring1A and Ring1B, also known as Ring1 and Rnf2, respectively – Mouse Genome Informatics) and Polyhomeotic (Phc1, Phc2 and Phc3). Recent studies demonstrate that mono-ubiquitylation of histone H2A at lysine 119 is important in PcG-mediated silencing, with Ring1A/B functioning as the E3 ligase in this reaction (de Napoles et al., 2004; Wang et al., 2004).

[1]RIKEN Research Center for Allergy and Immunology, and [2]RIKEN Genomic Sciences Center, 1-7-22 Suehiro, Tsurumi-ku, Yokohama 230-0045, Japan. [3]Swammerdam Institute for Life Sciences, University of Amsterdam, Kruislaan 406, 1098 SM Amsterdam, The Netherlands. [4]RIKEN Center for Developmental Biology, 2-2-3 Minatojima-minamimachi, Chuo-ku, Kobe, Hyogo 6500047, Japan. [5]Developmental Epigenetics Group, MRC Clinical Sciences Centre, ICFM, Hammersmith Hospital, DuCane Road, London W12 ONN, UK. [6]Centro de Investigaciones Biologicas, Department of Developmental and Cell Biology, Ramiro de Maeztu 9, 28040 Madrid, Spain.

*Author for correspondence (e-mail: koseki@rcai.riken.jp)

**Accepted 29 January 2008**

Mouse and human ES cells have recently been analyzed by genome-wide ChIP, and PRC1 and PRC2 have been shown to repress genes involved in processes including development, transcriptional regulation and morphogenesis, via direct interactions with target genes (Boyer et al., 2006; Lee et al., 2006). Notably, PRC2 has been shown to share target genes with OCT4, SOX2 and/or NANOG in human ES cells (Lee et al., 2006). However, it is still unclear whether PcG and the core transcription network are functionally linked to regulate expression of their target genes.

In this study, we addressed the role of PRC1 in mouse ES cell maintenance and its functional interaction with the core transcriptional regulatory circuitry. We find that PRC1 is essential for the maintenance of ES cell identity and for the repression of developmental regulators by inhibiting chromatin remodeling. We go on to show that Ring1A/B-mediated PcG silencing is Oct3/4-dependent, whereas it is abolished by developmental cues resulting in *Gata6* activation. Collectively, our data suggest that Ring1A/B-mediated Polycomb silencing functions downstream of the core transcriptional regulatory circuitry to maintain ES cell self-renewal.

## MATERIALS AND METHODS

### Mouse cells

*Eed*-KO, *Dnmt1*-KO, *Oct3/4* conditional KO (ZHBTc4) ES cell lines and the ES cell line expressing a Gata6-GR fusion (G6GR) were described previously (Azuara et al., 2006; Lei et al., 1996; Niwa et al., 2000; Shimosato et al., 2007). Generation of mutant *Ring1A* and *Ring1B* flox alleles were described previously (Cales et al., 2008; del Mar Lorente et al., 2000). *Rosa26*::*CreERT2* transgenic mice were purchased from Artemis Pharmaceuticals (Seibler et al., 2003). *Ring1A*$^{-/-}$;*Ring1B*$^{fl/fl}$;*Rosa26*::*CreERT2* ES cells were derived from blastocysts. Male ES cells were used in this study.

### Immunoprecipitation (IP) and chromatin immunoprecipitation (ChIP) analyses

IP (Isono et al., 2005a) and ChIP (Orlando et al., 1997) were performed as previously described. Immunoprecipitated and input DNA were quantified by real-time PCR. Primer and probe sequences are available upon request. Antibodies used in this study are listed in Table 1.

### Reverse transcription and quantitative real-time PCR

RNA extraction and cDNA synthesis were performed as described previously (Isono et al., 2005b). Quantitative real-time PCR was carried out using the SYBR Green (Stratagene, Agilent Technologies, Santa Clara, CA) or Taqman (Biosearch Technologies, Novato, CA) method and amplifications detected with an Mx3005P (Stratagene, La Jolla, CA). Primer and probe sequences are available upon request.

### Microarray methods and data analysis

Total RNA was extracted using Trizol (Invitrogen, Carlsbad, CA) and purified with RNeasy separation columns (Qiagen, Hilden, Germany). First-strand cDNA was synthesized and hybridized to Affymetrix GeneChip Mouse Genome 430 2.0 arrays (Affymetrix, Santa Clara, CA) to assess and compare the overall gene expression profiles.

To obtain normalized intensities from at least two slides, the quantile normalization method was used for every feature on the array (Bolstad et al., 2003). We calculated the log of the ratio of intensity in the knockout (KO) samples to the intensity in the respective control samples. Probes were not applied for further analysis when signals were at insignificant levels in control and KO samples. The expression change of a gene was calculated using the geometric mean of all probes aligned on the gene.

The microarray and ChIP-chip data are available in the NCBI Gene Expression Omnibus (GEO) under the series GSE10573 [NCBI GEO] with sample accession numbers GSM265040 to GSM265045, GSM266065 to GSM266067, GSM266076, GSM266077, GSM266115, GSM266837 and GSM266838.

### Comparable expression analyses between KO ES cells

We obtained Pearson product-moment correlation coefficients of the logarithms of expression changes between respective KO ES cells. The 95% confidence intervals of correlation coefficients were calculated using Z transformation. Eigenvalues and eigenvectors of the distribution in scatter diagrams were calculated using principal component analysis with software R (http://www.r-project.org/).

### Gene ontology (GO) analysis

We performed GO analysis using our in-house programs written in Python and C++ and GO data retrieved from the Gene Ontology database (http://www.geneontology.org), KEGG (http://www.genome.jp/kegg/) and others (Auernhammer and Melmed, 2000; Heinrich et al., 2003). The version of the dataset used was Oct 27th, 2006, submitted by Mouse Genome Informatics (MGI). We aligned microarray probes on mouse genes and assigned GO terms on all probes using these alignments. The significance of each GO term was determined using Fisher's exact test and Bonferroni adjustment for multiple testing. The *P*-value reflects the likelihood that we would observe such enrichment or higher by chance. Subsequent statistical examinations were also conducted using Fisher's exact test.

### ChIP-chip experiment, assignment of IP regions and calculation of fold enrichment

ChIP-on-chip analysis of Ring1B binding was carried out using the Mouse Promoter ChIP-on-chip Microarray Set (G4490A; Agilent Technologies). ES cells were subjected to ChIP assay using anti-Ring1B antibody as described (Fujimura et al., 2006). Purified immunoprecipitated and input DNA were subjected to blunt ligation with linker oligo DNA, linker-

**Table 1. Antibodies used in this study**

| Target protein | Species and clonality | Experiment | Source/reference |
|---|---|---|---|
| Oct3/4 | Mouse monoclonal (C-10) | WB, IP | Santa Cruz (sc-5279) |
| Oct3/4 | Goat polyclonal | ChIP | Santa Cruz (sc-8628X) |
| Ring1B | Mouse monoclonal (#3) | WB, IP, ChIP | (Atsuta et al., 2001) |
| Phc1 | Mouse monoclonal | WB, ChIP | (Miyagishima et al., 2003) |
| Mel18 | Goat polyclonal | WB | Abcam (ab5267) |
| Cbx2 | Mouse monoclonal (2C6) | WB | (Fujimura et al., 2006) |
| Rybp | Rabbit polyclonal | WB | (Garcia et al., 1999) |
| Eed | Mouse monoclonal (M26) | WB, ChIP | (Hamer et al., 2002) |
| Suz12 | Mouse monoclonal (4F7) | WB | Made in our laboratory |
| Ezh2 | Mouse monoclonal (M10) | WB | (Hamer et al., 2002) |
| Acetylated histone H3 | Rabbit polyclonal | WB, ChIP | Millipore/Upstate (06-599) |
| Trimethylated histone H3-K4 | Rabbit polyclonal | WB, ChIP | Millipore/Upstate (07-473) |
| Trimethylated histone H3-K27 | Rabbit polyclonal | WB, ChIP | Millipore/Upstate (07-449) |
| Ubiquitylated histone H2A | Mouse monoclonal (E6C5) | WB | Millipore/Upstate (05-678) |
| RNA polymerase II | Mouse monoclonal (8WG16) | ChIP | Millipore/Upstate (05-952) |
| Lamin B | Goat polyclonal | WB | Santa Cruz (sc-6216) |

WB, western blot; IP, immunoprecipitation; ChIP, chromatin immunoprecipitation.

mediated PCR (LM-PCR), labeling, hybridization and washing following the Agilent mammalian ChIP-on-chip protocol. Scanned images were quantified with Agilent Feature Extraction software under standard conditions.

Assignment of regions bound by Ring1B around transcription start sites (TSSs) was carried out using direct sequence alignment on the mouse genome database (NCBI version 36). The location of Ring1B-bound regions was compared with a set of transcripts derived from the MGI database. We assigned bound regions that were within –8 kb to +2 kb of the TSS. Alignments on mouse genome and TSSs of genes were retrieved from Ensembl (http://www.ensembl.org).

The measured intensity ratios (IP/input: fold enrichment) were calculated, and the maximum value of the ratios in each promoter region (–8 kb to +2 kb around TSS) of a gene was used to represent the fold enrichment of the gene. Fold enrichment was calculated only for probes whose signals both from IP and input DNAs were significant ($P<10^{-3}$).

## RESULTS

### Ring1A/B are required for the maintenance of ES cell identity

To investigate the role of PRC1 for maintenance of mouse ES cell identity, it was necessary to generate *Ring1A/B* double-knockout (dKO) ES cells because *Ring1B* single-knockout (*Ring1B*-KO) ES cells can be cultured for >20 passages and exhibit ES cell morphology (de Napoles et al., 2004; Fujimura et al., 2006) (data not shown). Thus, we established *Ring1A*$^{-/-}$;*Ring1B*$^{fl/fl}$;*Rosa26*::*CreERT2* ES cell lines, in which *Ring1B* could be conditionally deleted by 4-hydroxy tamoxifen (OHT) treatment. Ring1B protein levels were dramatically depleted within 48 hours of OHT administration (Fig. 1A), and loss of Ring1B resulted in reduced levels of other PRC1 components Mel18, Phc1/2 and Cbx2 (Fujimura et al., 2006; Leeb and Wutz, 2007). At a global level, PRC1-regulated mono-ubiquitylated histone H2A (H2Aub1) was rapidly depleted within 48 hours following OHT treatment (Fig. 1B). We thus concluded that PRC1 could be conditionally depleted in this ES cell line by OHT.

In the *Ring1A/B*-dKO, in contrast to the *Ring1B*-KO ES cells, proliferation was halted and the cells gradually lost typical ES cell morphology after OHT administration (Fig. 1C). Moreover, genome-wide mRNA analysis revealed preferential derepression of genes involved in differentiation and/or developmental processes (Fig. 1D; see also Table S1 in the supplementary material). These observations, considered together with structural and biochemical similarities of Ring1A and Ring1B (Buchwald et al., 2006), led us to hypothesize a compensatory role of Ring1A for Ring1B in the repression of developmental genes in ES cells. This idea is partly supported by the increased expression of Ring1A protein observed in the *Ring1B*-KO ES cells (see Fig. S1 in the supplementary material). We first compared gene expression between the *Ring1A/B*-dKO and *Ring1B*-KO ES cells by microarray analyses. We found that 491 genes were derepressed more than 2-fold in *Ring1B*-KO (constitutive), whereas in *Ring1A/B*-dKO (day 4) ES cells, 999 genes were derepressed (see Table S2 in the supplementary material). Fold expression changes for respective probes in *Ring1A/B*-dKO and *Ring1B*-KO ES cells, determined against the parental or wild-type cells, were plotted on a scatter diagram and the correlation was calculated according to Pearson (see Fig. S2 in the supplementary material). We found a strong correlation ($r$=0.386) in total calculable genes (see Fig. S2 in the supplementary material). This result indicates significant overlap of genes derepressed in *Ring1A/B*-dKO and *Ring1B*-KO ES cells. The level of derepression was much higher in *Ring1A/B*-dKO than in *Ring1B*-KO ES cells, as represented by differences in variance (see Fig. S2 in the supplementary material). On average, developmental genes were 1.389-fold derepressed in *Ring1A/B*-dKO ES cells, but 1.046-fold in *Ring1B*-KO (see Table S3 in the supplementary material). We confirmed these quantitative differences by evaluating the expression levels of several developmental regulators including *Gata6* and *Cdx2* by quantitative RT-PCR. These genes were significantly derepressed by conditional depletion of Ring1B, but the degree of derepression was higher in the *Ring1A/B*-dKO than in the *Ring1B*-KO cells (Fig. 1E). Therefore, Ring1A and Ring1B appear to act in a compensatory manner to repress the expression of developmental regulators in ES cells and consequently contribute to the maintenance of ES cells in an undifferentiated state. The phenotypic differences between *Ring1B*-KO and *Ring1A/B*-dKO ES cells are likely to be due to exaggerated derepression of developmental regulators such as *Gata6* and *Cdx2* in the dKO cells.

We next examined whether the derepression of developmental regulators is accompanied by disruption of the core transcriptional regulatory circuitry in ES cells. We performed multicolor immunofluorescence analysis for Oct3/4 and for Gata4, which is also expressed in primitive endoderm. Oct3/4 was expressed relatively uniformly in all of the control cells and Gata4 was also expressed in most of the cells (Fig. 1F, upper panels). Four days after OHT administration, we found striking heterogeneity in Oct3/4 expression (Fig. 1F, lower panels). In the example illustrated, most of the cells are compacted; however, a subset of cells at the edge spread out from the colony and exhibit epithelial cell morphology. Most of these cells expressed Gata4 but not Oct3/4 (Fig. 1F, arrowheads in lower right panel), which is likely to be indicative of the onset of spontaneous differentiation. Taken together with the gene expression analysis, these results indicate that Ring1A/B contribute crucially to the repression of ES cell differentiation and therefore to the maintenance of ES cell identity.

### Ring1A/B mediate repression of developmental regulators by inhibiting chromatin remodeling via direct binding

We next used ChIP analysis to determine whether genes derepressed in *Ring1A/B*-dKO ES cells were direct targets of PRC1. As shown in Fig. 2A, we observed binding of Ring1B and Phc1, another component of PRC1, to *Hoxb8*, *Gata6*, *Cdx2*, *Zic1* and *T*, all of which are derepressed in the *Ring1A/B*-dKO (Fig. 1E). Binding to all these genes was significantly reduced 2 days after administration of OHT in *Ring1A*$^{-/-}$;*Ring1B*$^{fl/fl}$;*Rosa26*::*CreERT2* ES cells, suggesting that Ring1B is essential for the establishment of PRC1 at their respective loci.

We next examined whether genes derepressed in *Ring1A/B*-dKO ES cells were bound by Ring1B at their promoters using a ChIP-chip approach (Fig. 2B; see Tables S4 and S5 in the supplementary material). We identified almost the same set of Ring1B targets that had been reported previously, if a certain threshold is adopted to distinguish genes bound by Ring1B (Boyer et al., 2006) (data not shown). We further clarified linear correlations between the degree of Ring1B binding and derepression in *Ring1B*-KO and *Ring1A/B*-dKO ES cells (Fig. 2B). These results indicate that Ring1A/B generally repress transcription by directly binding to the target loci in a dose-dependent manner.

Recent studies have demonstrated that PcG targets in ES cells are often characterized by a unique chromatin configuration, being simultaneously enriched for histone modifications associated with gene activity [histone H3 lysine 4 trimethylation (H3K4me3) and lysine 9/14 acetylation (H3Ac)] and modifications associated with PcG-mediated repression [specifically H3K27 trimethylation

(H3K27me3)] (Azuara et al., 2006; Bernstein et al., 2006). With this in mind, we investigated changes in chromatin configuration upon Ring1A/B depletion. At a global level, PRC1-mediated H2Aub1 was rapidly depleted (Fig. 1B). By contrast, there was no detectable change in overall levels of either H3K4me3, H3Ac, H3K27me3 or PRC2 components (see Fig. S3 in the supplementary material). We then analyzed promoter regions of selected PcG target loci derepressed in *Ring1A/B*-dKO ES cells by ChIP. In addition to histone modifications, we analyzed binding of Eed and non-phosphorylated RNA polymerase II (RNAPII) (Fig. 2C). Levels of H3Ac, H3K4me3 and RNAPII binding were significantly increased, whereas those of Eed and H3K27me3 were decreased. Although the molecular mechanism for the decrease in Eed binding upon Ring1A/B depletion is unclear, it is possible that changes in chromatin structure caused by Ring1A/B depletion might secondarily affect Eed binding.

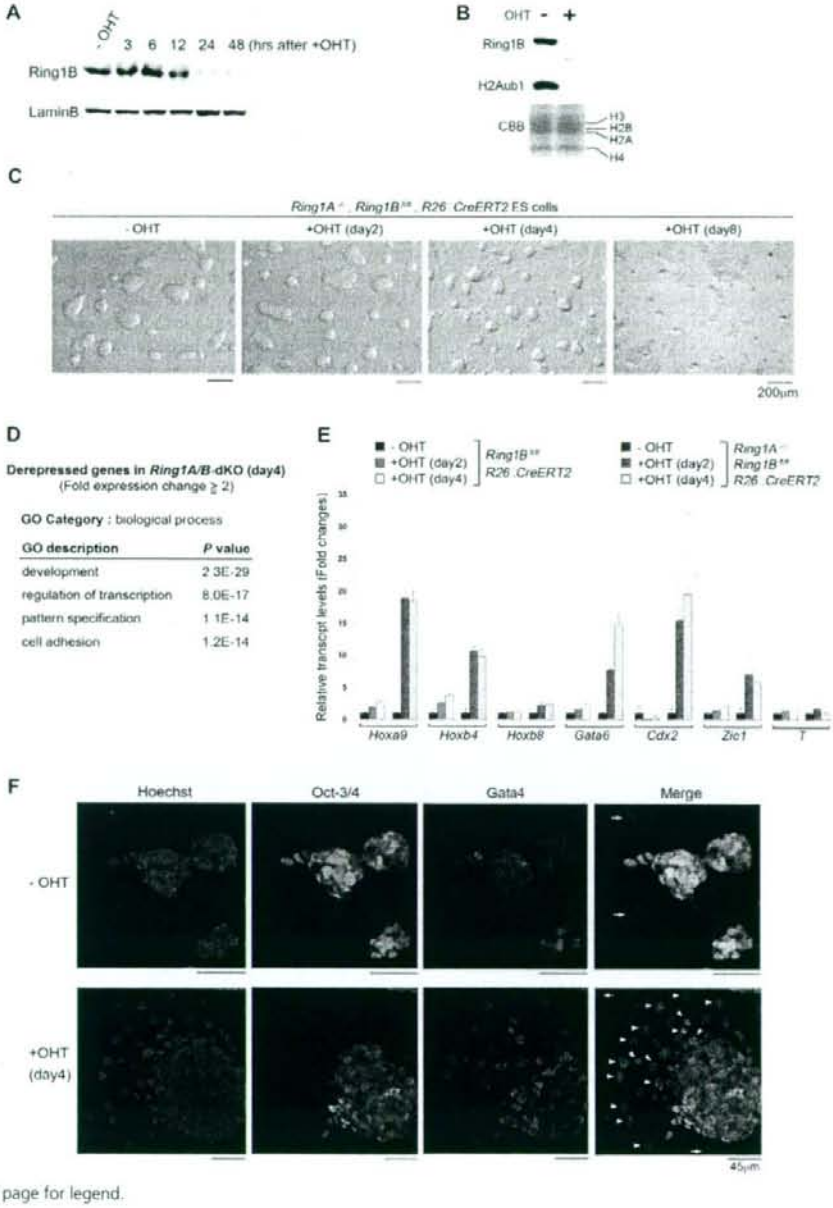


**Fig. 1.** See next page for legend.

**Fig. 1. Ring1A/B are required for the maintenance of mouse ES cell identity.** (**A**) Western blot analysis showing the kinetics of Ring1B depletion at 0, 3, 6, 12, 24 and 48 hours after treatment of *Ring1A*$^{-/-}$;*Ring1B*$^{fl/fl}$;*Rosa26*::*CreERT2* ES cells with 4-hydroxy tamoxifen (OHT). Lamin B served as a loading control. (**B**) Western blot showing Ring1B and mono-ubiquitylated H2A (H2Aub1) depletion 2 days after treatment with OHT in *Ring1A*$^{-/-}$;*Ring1B*$^{fl/fl}$;*Rosa26*::*CreERT2* ES cells. OHT was present in (+) or absent from (–) the ES cell culture medium. Coomassie Brilliant Blue (CBB) staining for histones was used as a loading control. (**C**) Morphology of conditional *Ring1A/B*-dKO ES cells. *Ring1A*$^{-/-}$;*Ring1B*$^{fl/fl}$;*Rosa26*::*CreERT2* ES cells were cultured in the absence (–OHT) or presence (+OHT) of OHT, which represent the single *Ring1A*-KO or *Ring1A/B*-dKO cells, respectively. At day 2, *Ring1A/B*-dKO ES cells retain ES-cell-like morphology; however, from day 3-4, *Ring1A/B*-dKO ES cells begin to lose ES-cell-like morphology. (**D**) Gene ontology (GO) analysis of genes more than 2-fold derepressed 4 days after OHT treatment of *Ring1A*$^{-/-}$;*Ring1B*$^{fl/fl}$;*Rosa26*::*CreERT2* ES cells. The significance (*P*-value) of the enrichment of each GO term is indicated for each category of biological process. For details, see Table S1 in the supplementary material. (**E**) Changes in expression levels of *Hoxa9*, *Hoxb4*, *Hoxb8*, *Gata6*, *Cdx2*, *Zic1* and *T* at 2 and 4 days after OHT treatment (+OHT) of *Ring1B*$^{fl/fl}$;*Rosa26*::*CreERT2* or *Ring1A*$^{-/-}$;*Ring1B*$^{fl/fl}$;*Rosa26*::*CreERT2* ES cells as determined by real-time PCR. Expression levels were normalized to an *Actb* control and are depicted as fold changes relative to the OHT-untreated (–OHT) ES cells. Error bars are based on the s.d. as derived from triplicate PCR reactions. (**F**) *Ring1A*$^{-/-}$;*Ring1B*$^{fl/fl}$;*Rosa26*::*CreERT2* ES cells were cultured in the absence (–OHT, upper panels) or presence (+OHT, day 4, lower panels) of OHT, and were immunostained with antibodies to Oct3/4 (green) and Gata4 (red). The left-most panels show nuclei stained with Hoechst 33342 (blue); the right-most panels show merged images. Arrowheads indicate differentiated cells that express Gata4 but not Oct3/4. Arrows indicate feeder cells. Scale bars: 200 μm in C; 45 μm in F.

The above results demonstrate that Ring1A/B depletion converts the local chromatin from an inactive into an active configuration. This would suggest that the engagement of PRC1 is important to ensure robust silencing within chromatin domains that are predisposed to transcriptional activation (Azuara et al., 2006; Bernstein et al., 2006).

## A large number of genes are repressed by both Ring1A/B and Oct3/4

Given that Ring1A/B are required for the maintenance of ES cell identity, we next examined the relationship between Ring1A/B and the core transcriptional regulatory circuitry in ES cells, because a previous study demonstrated that OCT3/4, SOX2 and NANOG co-occupy a significant subset of PRC2 target genes in human ES cells (Lee et al., 2006). In fact, inactive genes bound by OCT3/4, SOX2 and/or NANOG in human ES cells are overrepresented among those genes more than 2-fold derepressed in *Ring1A/B*-dKO mouse ES cells (see Fig. S4 in the supplementary material).

To directly test whether Ring1A/B mediate transcriptional silencing by the core transcriptional circuitry we made use of *Oct3/4* conditional knockout ES cells (ZHBTc4) (Niwa et al., 2000), comparing changes in gene expression in *Oct3/4*-KO and *Ring1A/B*-dKO cells. Because most *Oct3/4*-KO ES cells begin to exhibit trophectoderm-like morphology within 2 to 3 days after induction (Niwa et al., 2000), we analyzed RNA from ES cells 1 day after tetracycline (Tc) treatment, at which time Oct3/4 protein is extensively depleted, thus minimizing the contribution of secondary changes in gene expression resulting from differentiation. As controls, we also analyzed gene expression in *Eed*- and *Dnmt1*-KO ES cells. *Dnmt1*-KO ES cells self-renew but fail to undergo differentiation upon induction (Lei et al., 1996). Fold changes for respective probes determined against the parental cells were distributed on scatter diagrams and the correlation among respective KO ES cells was calculated (Fig. 3A). We found a strong correlation in total calculable genes between *Oct3/4*-KO and *Ring1A/B*-dKO ES cells ($r$=0.279). Overall gene expression in *Ring1A/B*-dKO ES cells also exhibited a strong correlation ($r$=0.359) with the *Eed*-KO, which might represent functional engagement of PRC1 and PRC2. By contrast, we found no correlation of the *Dnmt1*-KO with either the *Ring1A/B*-dKO ($r$=0.078) or *Oct3/4*-KO ($r$=–0.001). This analysis indicates that a large number of genes in ES cells are concurrently repressed by Oct3/4 and Ring1A/B.

Next we tested which genes regulated by Oct3/4 and Ring1A/B are important in maintaining ES cell identity. For this purpose, we extended the comparative gene expression analysis into sorted genes based on GO term categories. We found a comparable correlation in genes involved in regulation of transcription, transcription, development and apoptosis (Fig. 3B). Notably, the highest correlation was seen in genes involved in signaling pathways for Notch and Lif, both of which are implicated in stem cell maintenance (Androutsellis-Theotokis et al., 2006; Williams et al., 1988).

To test whether this observed correlation is statistically significant, we investigated the average expression changes caused by Ring1A/B depletion in genes more than 2-fold derepressed and repressed by Oct3/4 depletion. We further estimated the correlation of the expression changes with the degree of Ring1B binding to the respective genes. On average, derepressed genes in *Oct3/4*-KO cells were significantly derepressed in the *Ring1A/B*-dKO, as represented by a value at the zero point on the $x$-axis ($P$=1.23×10$^{-39}$) (Fig. 3C, red circle; see also Table S6 in the supplementary material). The degree of derepression in *Ring1A/B*-dKO showed a linear correlation with the degree of Ring1B binding (Fig. 3C, red circles). Concordantly, 120 out of 670 genes repressed by Oct3/4 were bound by Ring1B (Fig. 3D). By contrast, repressed genes in the *Oct3/4*-KO were only slightly repressed in the *Ring1A/B*-dKO, and these were genes that bound less Ring1B, whereas this was not the case at genes bound by Ring1B at intermediate or high levels (Fig. 3C, blue circles). Taken together with the spontaneous differentiation observed in *Ring1A/B*-dKO ES cells, Ring1A/B appear to be functionally linked with Oct3/4 in mediating ES cell identity.

## Oct3/4 is required to engage PRC1 and PRC2 at target gene promoters

To examine the molecular basis for the functional link between Oct3/4 and Ring1A/B, we used ChIP to investigate the effect of Oct3/4 deletion on the levels of Ring1B at selected targets bound by both Ring1B and Oct3/4 and/or Nanog (Boyer et al., 2005; Loh et al., 2006). Of the selected genes *Cdx2*, *Hand1*, *Gata6* and *Hoxb4* were derepressed 1 day after Oct3/4 depletion, whereas *T*, *Otx2* and *Hoxb8* were not (Fig. 4A). Ring1B binding was significantly reduced irrespective of transcriptional status, suggesting Oct3/4-mediated regulation Ring1B binding to the chromatin (Fig. 4B). We extended the analysis to examine whether this hierarchical link is applicable to other Ring1B target genes by the ChIP-chip approach. As shown in Fig. 4C, Ring1B binding to the promoter regions of the target genes was, on average, significantly reduced 2 days after Tc treatment of ZHBTc4 ES cells. Therefore, binding of Ring1B to the chromatin in ES cells is generally dependent on Oct3/4. It has

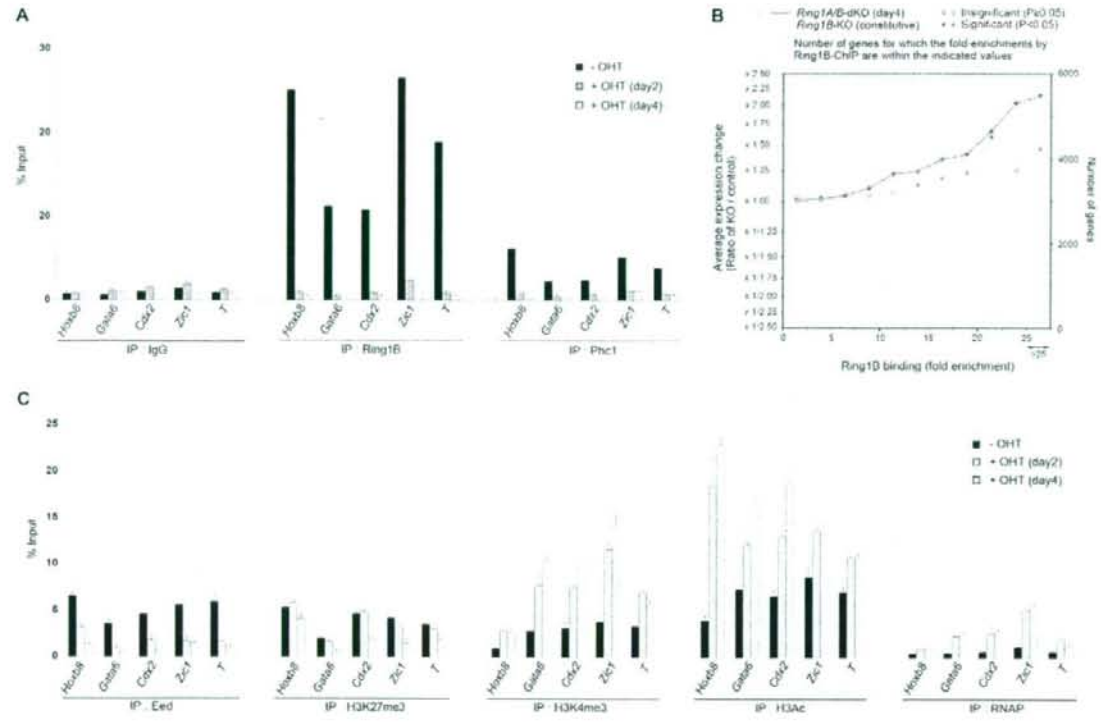


**Fig. 2. Ring1A/B mediate repression of developmental regulators by inhibiting chromatin remodeling via direct binding.** (**A**) Loss of Ring1B and Phc1 binding to the selected target promoter regions upon depletion of Ring1B in ES cells. Kinetics of local levels of Ring1B binding and Phc1 binding after OHT administration in *Ring1A*$^{-/-}$;*Ring1B*$^{fl/fl}$;*Rosa26*::*CreERT2* ES cells were determined by ChIP and site-specific real-time PCR. The relative amount of immunoprecipitated DNA is depicted as a percentage of input DNA. Error bars represent s.d. determined from at least three independent experiments. (**B**) Quantitative representation of the correlation between Ring1B binding and degree of derepression. Genes bound by Ring1B in their promoter regions in wild-type ES cells were identified by a ChIP-on-chip approach. Fold enrichment values for respective genes were calculated against the input and binned (each bin containing 2.5-fold enrichment). The number of genes in a bin (yellow bar) and the average change in expression from microarray analysis of *Ring1B*-KO (blue) and *Ring1A/B*-dKO (red) are indicated. Expression changes were statistically evaluated using Student's *t*-test under the null hypothesis that derepression was not observed. Significantly ($P<0.05$) derepressed bins and insignificant bins are indicated by solid and open circles, respectively. For actual values used to derive the graph and a list of Ring1B-bound genes, see Tables S4 and S5, respectively, in the supplementary material. (**C**) Changes in PRC2 binding and histone modification at Ring1B target loci following *Ring1A/B* depletion in ES cells. Kinetics of local levels of Eed, histone H3 lysine 27 trimethylation (H3K27me3), lysine 4 trimethylation (H3K4me3), lysine 9/14 acetylation (H3Ac), and non-phosphorylated RNA polymerase II (RNAPII) binding at the selected targets for Ring1B after OHT administration in *Ring1A*$^{-/-}$;*Ring1B*$^{fl/fl}$;*Rosa26*::*CreERT2* ES cells were determined by ChIP and site-specific real-time PCR. The relative amount of immunoprecipitated DNA is depicted as a percentage of input. Error bars represent s.d. determined from at least three independent experiments.

been reported that chromatin binding of Ring1B is also regulated by PRC2 functions (Boyer et al., 2006). We thus extended the analysis to address whether Oct3/4-dependent chromatin-binding of Ring1B involves PRC2, and found that binding of Eed to these genes was significantly reduced as well (Fig. 4B). Taken together, these results indicate that Oct3/4 mediates local engagement of PRC1 and PRC2.

Since enforced Ring1A/B depletion led to a rapid increase in the H3K4me3 level at the target genes (Fig. 2C), we next investigated changes in the degree of H3K4me3 at these genes upon Oct3/4 depletion. Notably, the level of H3K4me3 was increased at *Cdx2*, *Hand1*, *Gata6* and *Hoxb4*, whereas it was reduced or unchanged at *T*, *Otx2* and *Hoxb8*, consistent with increased gene expression (Fig. 4B). This indicates that the global reduction of PcG binding is not the sole mechanism for the changes in gene expression profile observed in ES cells upon Oct3/4 depletion. Oct3/4 has been suggested to upregulate some target genes and downregulate others. *Otx2* is one gene that has been experimentally verified to be upregulated directly by Oct3/4 (Boyer et al., 2005; Loh et al., 2006; Matoba et al., 2006). Moreover, the co-occupancy of promoters by PRC2 and OCT4/SOX2/NANOG has been demonstrated only at the transcriptionally repressed genes in human ES cells (Boyer et al., 2006). Considered together with the phenotypic difference between *Oct3/4*-KO and *Ring1A/B*-dKO ES cells, the global reduction in PcG binding might be a part of the mechanism for the differentiation of *Oct3/4*-KO ES cells.

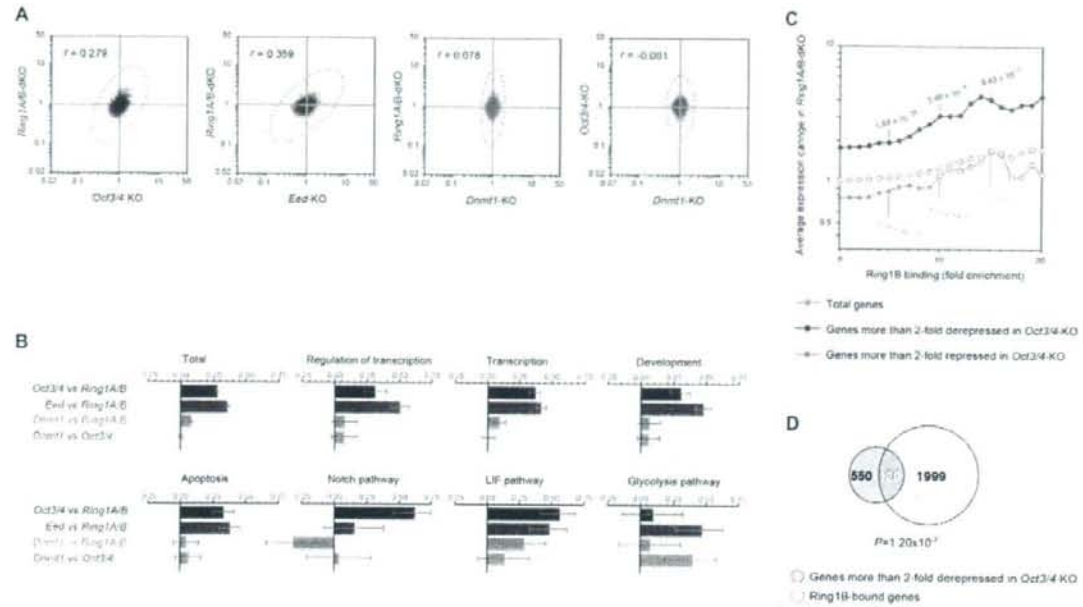


**Fig. 3. Significant overlap of derepressed genes in *Ring1A/B*-dKO and *Oct3/4*-KO ES cells.** (**A**) Scatter diagrams representing the correlation for changes in gene expression between respective KO ES cells. Each dot represents a specific probe. Fold changes of expression given by each probe in each KO against parental ES cells are dotted in the scatter diagram. Pearson's correlation coefficient (*r*) in each comparison is indicated in each panel. The distribution of dots is approximated by dotted ellipses. We prepared RNA from *Oct3/4*-KO ES cells 1 day after gene deletion was induced; *Ring1A/B*-dKO RNA was isolated at 4 days. Diagrams indicate the correlation of gene expression in *Eed*-KO versus *Ring1A/B*-dKO (green), *Oct3/4*-KO versus *Ring1AB*-dKO (red), *Dnmt1*-KO versus *Ring1A/B*-dKO (yellow), and *Dnmt1*-KO versus *Oct3/4*-KO (blue). (**B**) Pearson's correlation of expression changes for probes that belong to specific GO classifications are shown by bars. The same color codes are used as in A. Annotations are indicated above each graph. Error bars represent 95% confidence intervals of correlation coefficients calculated by Z transformation. (**C**) Graphical representation of correlation of derepressed genes in *Oct3/4*-KO and *Ring1A/B*-dKO ES cells in terms of the degree of Ring1B binding. Based on the genome-wide gene expression profiling, we first identified groups of genes more than 2-fold derepressed (red circles) or repressed (blue circles) in *Oct3/4*-KO ES cells. Average expression changes in *Ring1A/B*-dKO cells among those genes were plotted according to the degree of Ring1B binding determined by ChIP-chip and compared with the average of total genes (yellow circles). Where average expression changes in respective groups were statistically significant, relative to the total, the circles are solid; the open blue circles indicate that the difference from total genes is not statistically significant. *P*-values over 5-, 10- and 15-fold enrichment for Ring1B binding are shown. For actual values, see Table S6 in the supplementary material. (**D**) A significant fraction of the genes repressed by Oct3/4 is bound by Ring1B. The number of genes in each category of the Venn diagram is indicated.

Finally, we examined whether the binding of Oct3/4 depends on Ring1A/B. The levels of Oct3/4 binding to the PcG target sites were either unchanged or slightly decreased 2 to 4 days after OHT treatment of the *Ring1A/B*-dKO ES cells (Fig. 4D). Considering that the overall level of Oct3/4 decreases slightly 4 days after OHT treatment (see Fig. S3 in the supplementary material), we conclude that Ring1A/B are not directly required for the binding of Oct3/4 to the target sites.

In summary, loss of Oct3/4 consistently results in the reduction of Ring1B and Eed binding at PcG target genes in ES cells. Oct3/4 may maintain the repression of essential developmental regulators such as *Cdx2* and *Gata6* (Fujikura et al., 2002; Niwa et al., 2005) by maintaining local engagement of PRC1 and PRC2.

## Molecular links between Polycomb and the core transcriptional regulatory circuitry

To determine the molecular mechanism for the global reduction of Ring1B binding upon Oct3/4 depletion, we investigated the effect of Oct3/4 deletion on the level of PRC1 and PRC2 proteins. Although Ring1B expression was only minimally affected during the first 48 hours of Tc treatment, expression of Phc1, Eed and Suz12 was significantly reduced (Fig. 5A). The decrease in Phc1 and PRC2 proteins was accompanied by a significant reduction in their respective transcript levels, whereas this was not the case for other PRC1 components, including *Ring1B* and *Bmi1* (Fig. 5B). Therefore, Oct3/4 regulates the expression of PRC1 and PRC2 components, and this may partly involve transcriptional regulation.

We also investigated whether the physical interaction of Ring1B with the Rex1 (Zfp42 – Mouse Genome Informatics) complex (Wang et al., 2006) could be extended to Oct3/4. Significant amounts of Oct3/4 and Ring1B as well as Rybp, a Ring1B-binding protein (Garcia et al., 1999), were found to form complexes in ES cells, whereas the PRC2 protein Suz12 did not co-immunoprecipitate with either Oct3/4 or Ring1B (Fig. 5C). Since reciprocal co-immunoprecipitation of Oct3/4 and Ring1B was not affected by the addition of ethidium bromide, which is known to

disrupt protein-DNA interactions without affecting protein-protein interactions (Lai and Herr, 1992) (Fig. 5C, right), this interaction is not mediated by genomic DNA. This result suggests that the local binding of PRC1 to chromatin might involve direct interactions between PRC1 and protein complexes that include Nanog and/or Oct3/4. Taken together, these results suggest that PRC1 is linked to the core transcriptional regulatory circuitry at multiple levels.

## PRC1/2 binding is significantly reduced by Gata6 overexpression in ES cells

We went on to address whether PRC1/2 binding depends solely on Oct3/4 or on the regulatory system for ES cell self-renewal. Various differentiation cues have been demonstrated to disrupt ES cell self-renewal maintained by the core transcriptional regulatory circuitry. For example, Gata6 has been thought of as a downstream effector of Nanog, and enforced Gata6 expression induces the differentiation program towards extraembryonic endoderm (Chazaud et al., 2006; Fujikura et al., 2002). We therefore examined the effects of the enforced expression of Gata6 on PRC1/2 engagement at Ring1B targets using ES cells expressing a Gata6-GR fusion protein (G6GR) (Shimosato et al., 2007). As previously described, G6GR cells rapidly lose ES-cell-like morphology and show dispersed visceral endoderm-like morphology upon Gata6 activation by the administration of dexamethasone (Dex) (see Fig. S5 in the supplementary material).

We first analyzed the effect of Gata6 activation on the level of PRC1 and PRC2 proteins (Fig. 6A). The level of Ring1B protein was unaffected or only minimally affected during the first 2 days of Dex treatment, but was slightly decreased by day 3. The levels of Phc1, Ezh2, Eed and Suz12 proteins were significantly reduced after Dex treatment, whereas H3K27me3 was unaffected.

Next we used microarray analysis to evaluate the effect of enforced Gata6 expression on gene expression, and compared this profile with those of *Oct3/4*-KO and *Ring1A/B*-dKO ES cells. We found a comparable correlation between Gata6-differentiated and *Ring1A/B*-dKO ES cells ($r$=0.297), between *Oct3/4*-KO and Gata6-differentiated ES cells ($r$=0.318), and between *Oct3/4*-KO and *Ring1A/B*-dKO ES cells ($r$=0.279), not only in terms of total calculable genes but also in genes involved in development,

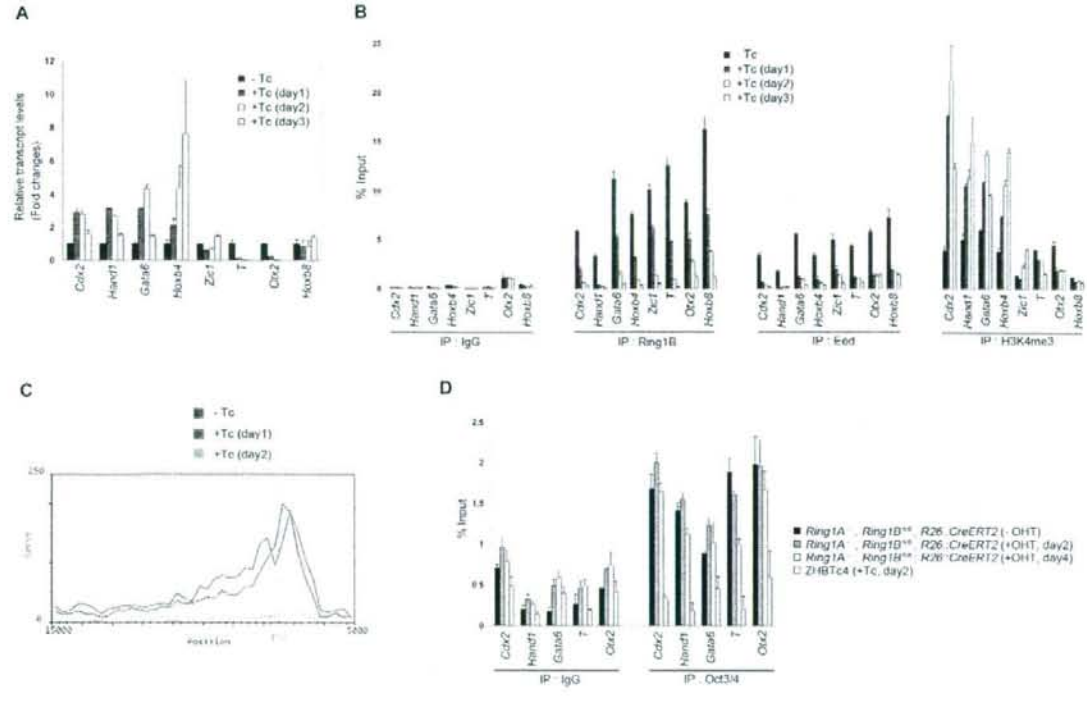


**Fig. 4. Oct3/4 is required to engage PRC1 and PRC2 at target gene promoters.** (**A**) Changes in expression levels for the selected Ring1B target genes after tetracycline treatment of ZHBTc4 ES cells were determined as described in Fig. 1E. (**B**) ChIP analysis showing binding of Ring1B and Eed and levels of H3K4me3 at the promoter regions of the selected target genes after tetracycline treatment of ZHBTc4 ES cells. The relative amount of immunoprecipitated DNA is depicted as a percentage of input. Error bars represent s.d. determined from at least three independent experiments. (**C**) ChIP-on-chip analysis showing the average Ring1B binding to the promoter regions (from –8 kb to +2 kb relative to the transcription start sites) of the target genes before and after conditional deletion of *Oct3/4*. (**D**) ChIP analysis showing binding of Oct3/4 at the promoter regions of the selected target genes after OHT treatment of *Ring1A*$^{-/-}$;*Ring1B*$^{fl/fl}$;*Rosa26::CreERT2* ES cells. The relative amount of immunoprecipitated DNA is depicted as a percentage of input. Error bars represent s.d. determined from at least three independent experiments.